

CIRCUIT AND BEHAVIORAL ANALYSIS OF KLINOTAXIS

IN *CAENORHABDITIS ELEGANS*

by

KATHRYN E. McCORMICK

A DISSERTATION

Presented to the Department of Biology
and the Graduate School of the University of Oregon
in partial fulfillment of the requirements
for the degree of
Doctor of Philosophy

September 2013

DISSERTATION APPROVAL PAGE

Student: Kathryn E. McCormick

Title: Circuit and Behavioral Analysis of Klinotaxis in *Caenorhabditis elegans*

This dissertation has been accepted and approved in partial fulfillment of the requirements for the Doctor of Philosophy degree in the Department of Biology by:

Dr. Patrick C. Phillips	Chairperson
Dr. Shawn R. Lockery	Advisor
Dr. William M. Roberts	Core Member
Dr. Janis C. Weeks	Core Member
Dr. Clifford Kentros	Core Member
Dr. Michael S. Wehr	Institutional Representative

and

Kimberly Andrews Espy	Vice President for Research and Innovation; Dean of the Graduate School
-----------------------	--

Original approval signatures are on file with the University of Oregon Graduate School.

Degree awarded September 2013

© 2013 Kathryn E. McCormick
This work is licensed under a Creative Commons
Attribution-NonCommercial-ShareAlike (United States) License.



DISSERTATION ABSTRACT

Kathryn E. McCormick

Doctor of Philosophy

Department of Biology

September 2013

Title: Circuit and Behavioral Analysis of Klinotaxis in *Caenorhabditis elegans*

The nervous system is a complex organ that functions in most metazoans to sense and respond to a constantly changing world. How the nervous system does this is a major focus of systems-level neuroscience. This dissertation investigates the neural basis of the sensorimotor transformation underlying a spatial orientation strategy in the nematode *Caenorhabditis elegans*. Motile organisms rely on spatial orientation strategies to navigate to environments that are conducive to organismal fitness and comfort, e.g. environments with the correct temperature, light level, or access to food and mates. As such, spatial orientation strategies as a class represent a key behavior common to most forms of life on earth.

To explore the behavioral mechanism used by *C. elegans* for spatial orientation, we designed and manufactured a microfluidic device that breaks the feedback loop between self-motion and environmental change by partially restraining the animal. The device takes advantage of laminar flow at small scale to provide distinct environments across the dorsoventral undulation that constitutes locomotion in this animal without using a physical barrier. This device allowed us to conclude that worms use the change in chemical concentration sensed between lateral extremes of the locomotion cycle to direct forward locomotion toward a favorable stimulus, an orientation strategy termed

klinotaxis.

We then investigated the neuronal basis of this behavior using laser ablation, calcium imaging, and optogenetic stimulation. We found a minimal neuronal network for klinotaxis to sodium chloride including the ASE, AIY, AIZ, and SMB neuron classes that displays left/right asymmetry across the sensory neuron, interneuron, and motor neuron levels. We extended these results by ablating other neurons that have been implicated in klinotaxis in other studies. Finally, we imaged the ASE neurons during klinotaxis in the microfluidic device and found that these neurons are active on the timescale of individual head swings. Additionally, we found anecdotal evidence that photostimulation of ASE neurons expressing the light sensitive ion channel Channel Rhodopsin (CHR2) is sufficient to stimulate klinotaxis behavior.

This dissertation includes previously published co-authored material.

CURRICULUM VITAE

NAME OF AUTHOR: Kathryn E. McCormick

GRADUATE AND UNDERGRADUATE SCHOOLS ATTENDED:

University of Oregon, Eugene
Bryn Mawr College, Bryn Mawr, Pennsylvania

DEGREES AWARDED:

Doctor of Philosophy, 2013, University of Oregon
Bachelor of Arts, Biology, 2005, Bryn Mawr College

AREAS OF SPECIAL INTEREST:

Neuronal Basis of Behavior

PROFESSIONAL EXPERIENCE:

Graduate Research Fellow, Department of Biology, University of Oregon, 2007-2013

Graduate Teaching Fellow, Department of Biology, University of Oregon, 2007-2008

GRANTS, AWARDS, AND HONORS:

National Research Service Award, Neuronal Analysis of Action Selection, NIH, 2010-2013

Travel Award, Women in Graduate Sciences, 2011

Buck Scholarship Award, Neural Systems and Behavior, MBL, 2009

PUBLICATIONS:

McCormick KE, Gaertner BE, Sottile M, Phillips PC, and Lockery SR (2011)
Microfluidic devices for analysis of spatial orientation behaviors in
Caenorhabditis elegans. *PLoS ONE* 6(10): e25710.

- Faumont S, Rondeau G, Thiele TR, Lawton KJ, McCormick KE, Sotille M, Griesbeck O, Heckscher ES, Roberts WM, Doe CQ, Lockery SR (2011) An image-free opto-mechanical system for creating virtual environments and imaging neuronal activity in freely moving *Caenorhabditis elegans*. *PLoS ONE*. 6(9):e24666.
- Ortiz CO, Faumont S, Takayama J, Ahmed HK, Goldsmith AD, Pocock R, McCormick KE, Kunitomo H, Iino Y, Lockery S, Hobert O (2009) Lateralized gustatory behavior of *C. elegans* is controlled by specific receptor-type guanylyl cyclases. *Curr. Biol.* 19(12) 996-1004.
- Lockery SR, Lawton KJ, Doll JC, Faumont S, Coulthard SM, Thiele TR, Chronis N, McCormick KE, Goodman MB, Pruitt BL (2008) Artificial Dirt: microfluidic substrates for nematode neurobiology and behavior. *J. Neurophysiol.* 99 (6) 3136-43.
- Brodfehrer PD, McCormick K, Tapyrik L, Albano AM, Graybeal C (2008) Activation of two forms of locomotion by a previously identified trigger interneuron for swimming in the medicinal leech. *Invertebrate Neuroscience* 8 (1) 31-39.

ACKNOWLEDGMENTS

First and foremost, I wish to express my sincere gratitude to Dr. Shawn Lockery, without whom this research project would not exist. Serge Faumont has also been indispensable, and I thank him for his understanding and patience. Special thanks are due to my dissertation advisory committee, whose guidance has never failed at critical junctures. I also thank the members of Team Ion 2007: Crystal Davey, Kelly Heinlein, Liesl McCormick, and Michael Kyweriga. I could not have persevered without your compassion. Dr. C, thanks for the perspective. Take this work and shove it up your axon. In addition, I thank Joe Hall for reminding me that there is much more to life than graduate school. This work was supported by a predoctoral National Research Service Award from the National Institute of Health.

To my patient husband, Joe.

TABLE OF CONTENTS

Chapter	Page
I. INTRODUCTION	1
II. MICROFLUIDIC DEVICES FOR ANALYSIS OF SPATIAL ORIENTATION BEHAVIORS IN SEMI-RESTRAINED <i>CAENORHABDITIS</i> <i>ELEGANS</i>	7
Introduction.....	7
Results.....	10
Discussion.....	21
Materials and Methods.....	24
Bridge.....	26
III. LEFT / RIGHT ASYMMETRY IN THE NEURAL NETWORK UNDERLYING KLINOTAXIS IN <i>CAENORHABDITIS ELEGANS</i>	27
Introduction.....	27
Results.....	29
Discussion.....	42
Materials and Methods	45
IV. KLINOTAXIS IN CONTEXT: BROADENING THE NETWORK AND RELATING TO FREELY MOVING WORMS.....	49
Main Text.....	49
Materials and Methods	60
V. CONCLUSION	63
REFERENCES CITED.....	65

LIST OF FIGURES

Figure	Page
CHAPTER II	
1. Design of the chemosensory device.....	12
2. Behavioral responses to step gradients in chemoattractant concentration.....	15
3. Behavioral responses to temporal steps in osmolarity.....	17
4. Design of the two-layer thermosensory device.....	18
5. Behavioral response to step gradients in temperature.....	21
CHAPTER III	
1. Analysis of klinotaxis behavior in an individual N2 worm.....	31
2. Klinotaxis bias scales with concentration difference.....	33
3. Minimal neural network underlying klinotaxis.....	36
4. Effects of ablation of ASE neurons.....	38
5. Effects of ablation and genetic manipulation of AIY neurons.....	39
6. Effects of ablation of AIZ neurons.....	41
7. Effects of ablation of SMB neurons.....	42
CHAPTER IV	
1. Extended neural network for klinotaxis.....	50

Figure	Page
2. Summary of ablation experiments during symmetrical stimulus	51
3. Summary of ablation experiments during asymmetrical stimulus.....	51
4. Calcium Imaging of ASER.....	56
5. Calcium Imaging of ASEL	57
6. Photostimulation of ASER.....	58
7. Modeling of worm tracks.....	59

CHAPTER I

INTRODUCTION

All living things need ways of sensing and responding to changing conditions in the world around them. Although unicellular organisms and many plants wondrously accomplish this without the help of specialized nerve cells, most motile multicellular organisms rely on neural circuits to respond fluidly to an external stimulus through an event known as a sensorimotor transformation. Sensorimotor transformation is a general term that refers to processes by which a sensory input that impinges on a sensory cell is relayed and transformed inside the nervous system until it produces an appropriate motor response.

One of the simplest examples of this process, the patellar reflex or knee-jerk response, does not involve a central brain at all, but is handled at the level of the spinal cord (Kandel et al., 2000). The quadricep muscle is stretched by a mallet hitting the patellar tendon to which the quadricep is attached. The sensory neurons embedded in the quadricep respond to the stretch with an action potential. These neurons relay the signal from the impinging sensation to the motor neurons via a synapse in the dorsal root ganglion of the spinal cord. The motor neuron then relays the signal to the muscle, through an excitatory synapse to the same quadricep in which the stretch was sensed, causing the muscle to contract and the lower leg to kick upward.

Sensorimotor transformations underlie many of the actions we take in this world.

When we catch a ball, we must watch its trajectory and make a prediction about where the ball will be in the future based on this visual input. Then we must move our muscles such that our hand will intersect the path that the ball will take. It is a testament to the processing power of the nervous system that we can do all this correctly even a small fraction of the time, and that some of us can do it consistently.

Because the sensorimotor transformations that underlie actions like catching a ball are so complex and take place deep within the primate brain, some neuroscientists have turned to the simpler actions of animals with more accessible nervous systems to discover general principles of this phenomenon. The nematode roundworm *Caenorhabditis elegans* was popularized for study during the 1970s because it has a simple, tractable nervous system that can nevertheless give rise to many complex and interesting behaviors (Brenner, 1974). *C. elegans* (or “the worm”) is a transparent hermaphrodite that matures, from egg to adult, in only three days (Hall and Altun, 2008). The mature nervous system consists of only 302 neurons that are uniquely identifiable from worm to worm by position and genetic expression profile (Bargmann and Avery, 1998; Hobert, 2004). The neuronal morphology and synaptic connections between neurons have been painstakingly characterized through thin-slice electron microscopy (White et al., 1986; Chen et al., 2006) . In addition, the worm readily expresses exogenous genes such as fluorescent proteins and calcium indicators (Chalfie et al., 1994; Kerr et al., 2000). These can be targeted to particular tissues by pairing the sequence for the exogenous gene with the promoter region for an endogenous gene that is restricted to the cell or tissue of

interest (for instance, a particular class of neuron or muscle). These and many other advantages make the worm a powerful organism for studying the neuronal basis of behavior.

Despite its relatively small size and simplicity, *C. elegans* must, like the rest of the metazoans on earth, solve problems related to living. Chief among these is finding food in the environment. Another is finding conditions that are favorable: the right humidity, temperature, light level, etc.. Most motile organisms must rise to the challenge of orienting themselves within the vast space of the Earth and navigating to preferred micro-environments. It is not surprising that some of the strategies that have been evolved to orient in space are shared across species.

The first thorough classification of strategies used for spatial orientation came in 1940 with the publication of “The Orientation of Animals: Kineses, Taxes, and Compass Responses” by Gottfried S. Fraenkel and D.L. Gunn. In it, they distinguish kineses, or undirected reactions, from taxes, or directed reactions. Bacteria such as *Escherichia coli* perform kinesis in the so called “biased random walk” spatial orientation strategy, wherein the organism “runs” (continues going forward) as long as conditions are improving in the environment, and “tumbles” (turns around to pick a random new direction) wherever conditions are deteriorating (Berg and Brown, 1972). In this way, a bacterium can spend most of its time in “good” places and avoid the “bad” places. *C. elegans* has a similar behavior that is termed in the literature the “pirouette mechanism,” and is most thoroughly characterized in reaction to sodium chloride (Pierce-Shimomura et al., 1999). The worms like salt in their environment, and will accumulate at regions of

high salt on an agar plate (Ward, 1973; Dusenbury, 1974). The pirouette mechanism is the most well-studied method that worms use to achieve this accumulation. When the salt concentration is increasing ($dC/dt > 0$), the animal's probability of going forward is high. When the salt concentration decreases ($dC/dt < 0$), forward probability drops and the worm is apt to reverse and head off in a new direction with the help of a behavioral sequence known as an "omega turn," in which the worm brings its head near its tail, briefly resembling the shape of an omega (Ω) (Croll, 1975 a,b). The combination of reversal and omega turn, or sometimes a series of short reversals, is collectively referred to as a pirouette (Pierce-Shimomura et al., 1999). Both the pirouette mechanism in worms and the biased random walk in bacteria would be classified by Fraenkel and Gunn (1940) as klinokinesis (klino here meaning bend or incline), because it depends upon a change in course.

However, worms also have a more efficient way of orienting to environmental cues. This behavior was first characterized by Iino and Yoshida (2009) and was termed the "weathervane strategy" because, like a weathervane pointing into the wind, during this behavior the worms direct their forward locomotion up a gradient. Iino and Yoshida (2009) confirmed that this was a directed taxis by showing that the curvature of the path the worms took during forward crawling was correlated with the bearing they had with respect to the salt gradient. Thus, in the formalized nomenclature of Fraenkel and Gunn (1940), the worms can perform taxes (or directed responses) as well as kinesis (or undirected responses) to orient to environmental cues. Taxes are of particular interest to study because they imply a more complex circuit-level architecture than do kineses.

Rather than always having the same response to the same stimulus, as is seen in a kinesis, taxis requires that an outside stimulus be paired with an internal state of the animal in order to select an appropriate action.

Let us consider in detail the instantiation of klinotaxis in *C. elegans*. *C. elegans* crawls on its side and generates thrust through dorsoventral undulations. The two nostrils are thus oriented orthogonal to the plane of locomotion, and are only 8 microns apart (Ward et al., 1975). This arrangement makes it unlikely that a comparison of the chemical environment between the two nares is used in this behavior. As the worm crawls, the nostrils are swung from side to side, sampling the chemical environment through a series of regular lateral deviations from the direction of translation. For illustration, suppose that a salt source has created a gradient in the substrate, and a worm is crawling perpendicular to it such that the salt source is to the worm's left from the point of view of the observer. When the worm crawls forward, it will, in the course of locomotion, sample the environment to the left of itself and to the right of itself with each undulation cycle. The worm must make a comparison of the intensity of the salt stimulus on the two sides of its body and couple that with a representation of its body posture. In other words, the worm must not only detect that the salt is higher in concentration on one side, but that it is higher on the left side. Then the worm must bias its undulations to enact a curve towards the left. If the point source of salt is to the right, the whole pattern must be reversed so that the worm curves in the opposite direction. Thus, the problem of klinotaxis in *C. elegans* represents an instance of action selection in simplified form.

C. elegans is not the only species to use a klinotaxis strategy for spatial orientation. Larvae of many fly species, including *Drosophila melanogaster*, are known to use the strategy (Gomez-Marin et al., 2010). *Euglena* species also use it, although their locomotion involves spiraling rather than undulation within a single plane (Fraenkel and Gunn, 1940). One study reports that nurse sharks use klinotaxis to locate prey (Mathewson and Hodgson, 1972). A recent paper shows that while humans typically use tropotaxis (i.e., comparison of intensities between nostrils) to follow a scent trail, they are still capable of following trails when the two-point sampling system is reduced to a single point through the use of nasal prisms (Porter et al., 2007). In this case, humans resort to the regular lateral deviations that are the hallmark of klinotaxis.

Chapter II of this dissertation was previously published with co-authors. Chapter III is a manuscript in preparation that will be co-authored and published with Dr. Shawn Lockery.

CHAPTER II

MICROFLUIDIC DEVICES FOR ANALYSIS OF SPATIAL ORIENTATION BEHAVIORS IN SEMI-RESTRAINED *CAENORHABDITIS ELEGANS*

This work was published in volume 6 of the journal PLoS ONE in October, 2011. Dr. Bryn Gaertner and myself performed the experiments herein. Dr. Matthew Sottile assisted in developing image processing software to analyze the data. Dr. Patrick Phillips and Dr. Shawn Lockery were the principle investigators and assisted with experimental design.

INTRODUCTION

The ability to migrate up or down chemical and thermal gradients is a key component of the spatial orientation behaviors from single-cell microorganisms (Alder, 1966) to humans (Porter et al., 2007). Such abilities – called chemotaxis and thermotaxis, respectively – are essential to biological processes as diverse as reproductive fertilization, development, the immune response, feeding, and habitat selection. Analysis of the behavioral mechanisms of chemotaxis and thermotaxis can be simplified by the use of step-like spatial or temporal gradients. Step gradients are advantageous because orientation responses in many organisms are triggered by detection of changes in sensory

input rather its absolute magnitude. Therefore, in the case of a step gradient, the effective stimulus is confined to a small region of space or time, making it easier to establish causal connections between stimuli and responses.

The formation of spatial and temporal step gradients can be challenging in the fluid environments in which many orientation behaviors are investigated. Spatial step gradients are problematic because they are rapidly degraded by antagonistic processes such as convection and diffusion, whereas temporal step gradients are problematic because of long switching times when perfusing macroscopic experimental chambers. At microfluidic scales, however, spatial step gradients are readily formed by combining laminar streams of distinct fluids (Jeon et al., 2000). This feature has led to the development of microfluidic step gradient generators for the study of spatial orientation behaviors in several types of widely used microorganisms including bacteria (Ahmed et al., 2010), paramecium (Giuffre et al., 2011), sperm cells (Koyama et al., 2006), and nematodes (Lockery et al., 2008; Albrecht and Bargmann, 2011). Temporal steps are also comparatively easy to generate in microfluidic devices because low fluid volumes lead to reduced switching times (Lockery et al., 2008; Albrecht and Bargmann, 2011).

In the current generation of microfluidic devices for studies of spatial orientation, organisms move freely within the device. Although beneficial in many respects, freedom of movement has two key limitations. First, freely moving microorganisms can be difficult to track, making longitudinal studies impractical. Second, in the case of spatial gradients, when, how often, and at what angle a particular individual encounters the step are uncontrolled random variables that depend entirely on the organism's behavior.

Analysis of orientation mechanisms would therefore be accelerated by a general method for presenting step gradients to semi-restrained individuals.

As a first step toward addressing this need, we sought to develop step-gradient devices for studying orientation behaviors in the nematode worm *Caenorhabditis elegans*. *C. elegans* is an unusually well-described organism that is widely used as a model system in biological and biomedical research (Riddle et al., 1997). Adults of this species are 1 mm long and 80 μm wide, making them large enough to be manipulated easily, yet small enough to be compatible with microfluidic devices (Ben-Yakar et al., 2009). In addition, *C. elegans* exhibits a diverse repertoire of spatial orientation behaviors including chemotaxis to gradients of soluble compounds and odorants (Bargmann, 2006), thermotaxis to preferred temperatures (Garrity et al., 2010), and avoidance of regions of high osmolarity (Culotti and Russell, 1978). Two main behavioral strategies have been proposed to explain spatial orientation behaviors in *C. elegans*. The first is a biased random walk, also known as klinokinesis, in which the frequency of large turns is modulated by the rate of change of attractant concentration (Pierce-Shimomura et al., 1999). The second is a directed strategy known as klinotaxis, in which the animal's course is continuously corrected toward the line of steepest ascent up the gradient (Iino and Yoshida, 2009). A necessary condition of klinotaxis is that course corrections occur as a result of alternating lateral displacements of the pertinent sensory organs (Fraenkel and Gunn, 1940). Neuronal analysis of these behaviors reveals universally applicable circuit motifs for behaviors in higher organisms (Lockery, 2011).

Here we describe a pair of microfluidic devices that reliably deliver step gradients in chemical concentration and temperature to semi-restrained *C. elegans*. The nematode is clamped at its midsection by a vacuum-assisted restraint aligned with the border between two laminar fluid streams. The head and anterior body, which are free to move, exhibit the side-to-side head swings characteristic of normal locomotory undulation in nematodes. The device is capable of delivering both spatial and temporal steps. To demonstrate the utility of these devices, we investigated the behavioral mechanisms of orientation to chemical, thermal, and osmotic gradients at the resolution of individual head swings in *C. elegans* for the first time. Using spatial steps, we found that locomotion is biased toward favored chemical and thermal conditions during individual head swings, supporting the hypothesis that *C. elegans* employs klinotaxis in both modalities. Using temporal steps, we found that worms transiently increase the probability of initiating avoidance responses following sudden changes in osmolarity, indicating that *C. elegans* may employ an unusual klinokinesis strategy to orient to osmotic cues. The device is readily adaptable to a wide range of studies including classical conditioning and neuronal imaging in intact, behaving animals.

RESULTS

Design of the chemosensory device

The chemosensory device consists of a Y-shaped channel formed in a single layer of PDMS bonded to a glass substrate (Fig. 1a,b). Solutions containing chemosensory stimulants enter via inlets located at the ends of each arm and are removed via an outlet at

the base of the stem. The solution flowing in each arm is selected manually by means of stopcocks attached to the fluid reservoirs (Fig. 1b), or automatically by a bank of solenoid valves (not shown); flow rate is regulated by a peristaltic pump attached to the outlet. The worm is positioned at the center of the Y where the fluids from the arms converge. We found that a simple passive clamp in the form of a channel with a narrow constriction was insufficient to prevent the worm from escaping from the device. This problem was solved by applying a vacuum to both sides of the worm via a manifold of 10 μm wide ports (Fig. 1c). The restraint immobilizes the middle third of the worm leaving the anterior (head) and posterior (tail) portions free to move. At the start of an experiment, the worm is captured in a fluid filled tube, inserted into the worm inlet, and positioned in the restraint; the vacuum is activated after the worm is in position.

The central feature of the design is that the two streams meet without mixing at the point of confluence. Thus, when the streams contain different concentrations of a chemical stimulus, a step-like chemical gradient is formed across the region in which the worm's anterior portion is free to move (Fig. 1d). Alternatively, the device can be used to deliver temporal concentration steps. This is done by flowing the same solution through both arms then simultaneously switching them to a different solution. We refer to these methods as the spatial and temporal modes of operation, respectively.

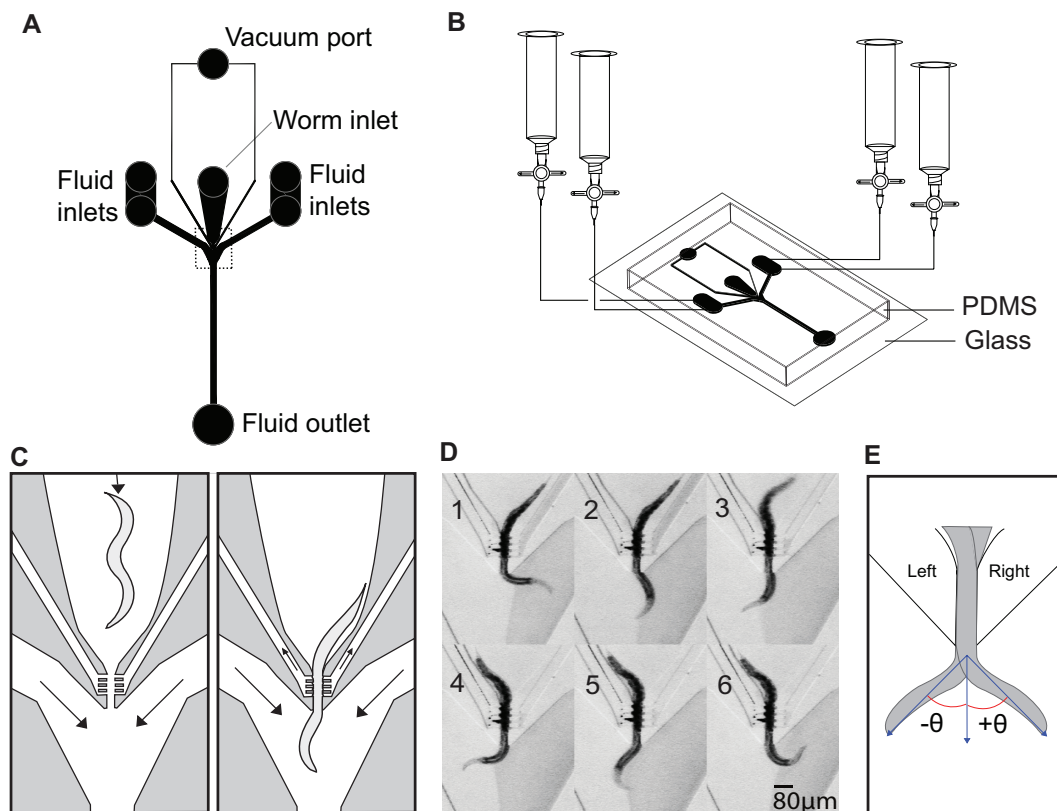


Figure 1. Design of the chemosensory device. (a) Top view showing the layout of channels, ports, inlets, and outlets. The region enclosed by the dashed rectangle is expanded in (c) and (d). (b) Perspective view showing the arrangement of fluid reservoirs and valves for switching fluids. (c) Schematic of the worm loading process. Arrows represent direction of flow in fluid and vacuum channels. Left panel: The worm is pushed toward worm restraint via a pressurized syringe (not shown) attached to worm inlet. Right panel: Once the worm is in place, an external vacuum source is applied and the syringe is de-pressurized. (d) Composite image with one stream dyed to demonstrate laminar flow during a complete head swing cycle. (e) Definition of head angle θ used for quantification of behavior. Undulations occur in the dorso-ventral plane. The terms “left” and “right” refer to the arms of the device.

Performance

Animal behavior. On an agar substrate, a freely crawling worm lies on its right or left side such that undulations occur in the dorso-ventral plane. We found that when inserted into the device, the worm invariably adopts such an orientation. We observed that the

anterior portion of the animal moved in a coordinated manner that qualitatively resembled the locomotion of unrestrained worms (Fig. 1d). Unrestrained worms exhibit two distinct modes of locomotion: crawling and swimming, which have undulation frequencies of ~ 0.8 Hz and ~ 2.1 Hz respectively (Pierce-Shimomura et al., 2008). Undulation frequency in the device was 0.34 ± 0.11 Hz ($n = 17$ worms, S.E.M.) suggesting that the worms were crawling rather swimming.

Temporal precision of stimulus delivery. To assess the chip's performance when being operated in temporal mode, we measured the time course of solution exchange. This was done by switching the flow in one of the arms from a clear solution to one containing an opaque substance (food dye) and measuring the time course of average luminance in a region of interest located near the convergence of the two streams. Solution exchange was complete in 0.53 ± 0.19 sec ($n = 5$ trials, s.e.m.) which is much shorter than the period of undulation in the device (2.9 sec).

Behavioral responses to step gradients in chemoattractant concentration

To demonstrate the new types of data that can be acquired by the chemosensory device, we first examined the behavioral mechanism of directed orientation responses in *C. elegans*. These responses are hypothesized to involve klinotaxis, i.e., modulations of head angle based on concentration changes sensed during the lateral component of head movements associated with individual undulations (Iino and Yoshida, 2009). However, this hypothesis is based on analysis of the trajectory of the nematode's centroid rather than detailed analysis of alterations in head swings that may be an essential component of

the orientation mechanism. To test the klinotaxis hypothesis at the resolution of individual head swings, we used the device in the spatial operating mode. This was done by subjecting individual worms to an alternating series of symmetrical and asymmetrical patterns of the attractant concentration (NaCl), in five contiguous epochs (Fig. 2a). Symmetrical stimulus epochs (either 10 mM or 0.001 mM NaCl) were interleaved with asymmetrical stimulus epochs (10 mM versus 0.001 mM NaCl) in a counterbalanced design. Behavior was quantified in terms of angular displacement θ of the tip of the worm's head as shown in Fig. 1e. Dorsoventral undulations continued throughout the experiment (Fig. 2b).

Data from individual worms showed that head swings from the high to the low concentration side in asymmetrical epochs were almost always truncated near the interface between the two solutions ($\theta = 0$), whereas this truncation was absent during symmetrical epochs, except immediately after switching to symmetrical solutions. Group data, in the form of ensemble averages of θ , showed that undulations were strongly biased toward the high concentration side (Fig. 2c,d; ANOVA with post hoc contrast, $p < 0.001$, $n = 17$). Average θ during symmetrical epochs was not significantly different from zero (post hoc contrast, $p > 0.05$, $n = 17$), indicating that the bias seen in asymmetrical epochs was specifically the result of the concentration differences presented. We conclude that *C. elegans* is capable of modulating head swings in response to concentration changes sensed during the lateral component of head movements, at least in the case of concentration changes on the order of 10 mM. This finding provides direct confirmation of the klinotaxis hypothesis.

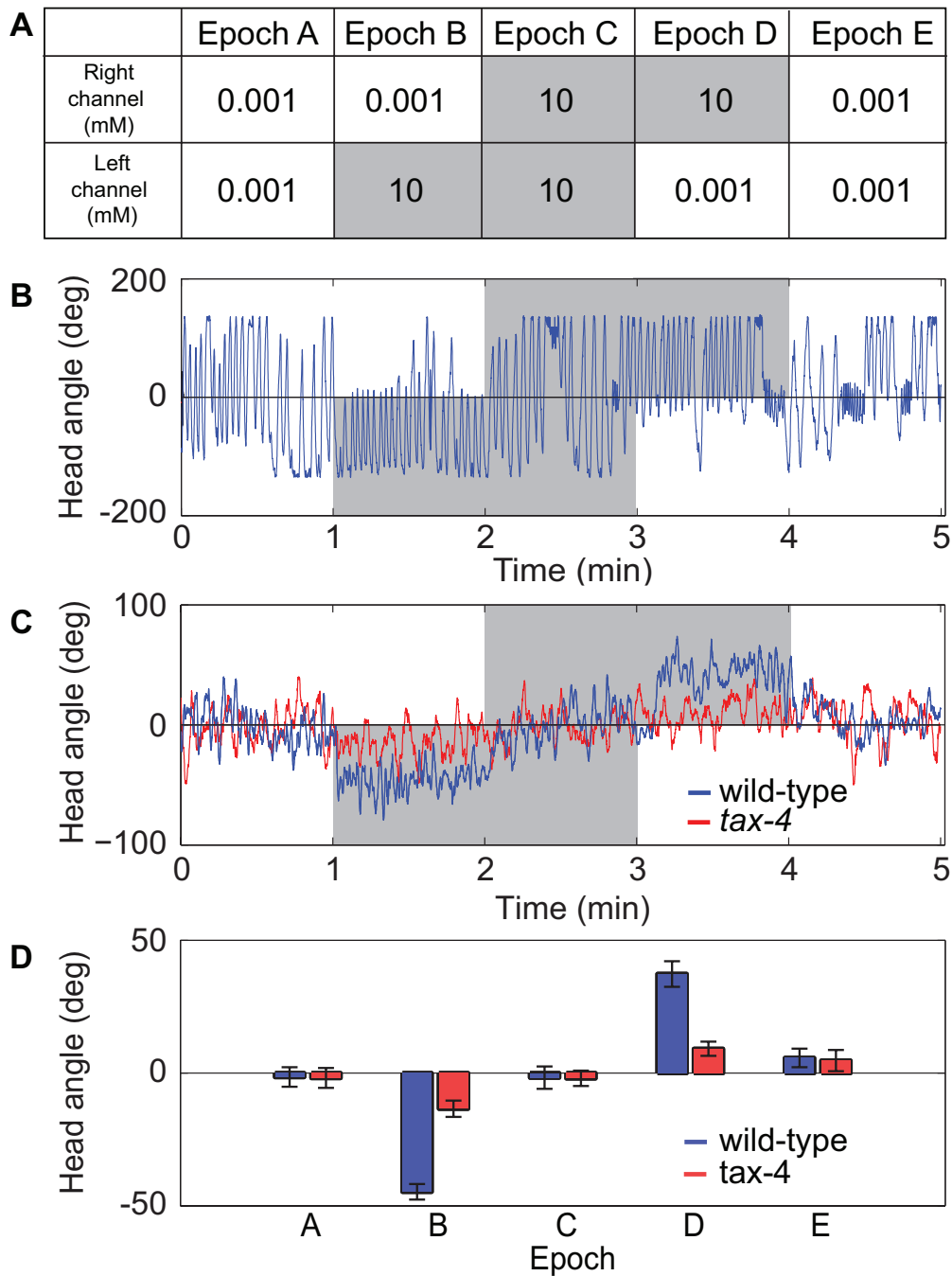


Figure 2. Behavioral responses to step gradients in chemoattractant concentration. (a) Stimulus protocol for chemosensory experiments. Values are the concentration of NaCl in mM. All epochs are one minute in length. Shading indicates timing and location of high concentration fluid. (b) Head angle versus time for a wild-type animal in response to the stimulus protocol in (a). (c) Ensemble averages of head angle for wild type animals and *tax-4* mutants. (d) Mean head angle of wild type animals and *tax-4* mutants by stimulus epoch for data shown in (c). Error bars are s.e.m.

Behavioral analysis of chemotaxis mutants is a powerful means of investigating the cellular and molecular basis of chemotaxis (Ben-Yakar et al., 2009). To demonstrate the ability of the chip to identify novel quantitative phenotypes in chemotaxis mutants, we examined the behavior of the mutant *tax-4*, which has a well characterized defect in chemotaxis (Dusenbery et al, 1975). This defect has been traced to impaired function of the TAX-4 protein, which is an ion channel subunit required for chemosensory transduction in *C. elegans* (Komatsu et al, 1996). We found that mean head angle during asymmetrical epochs was significantly reduced in the mutants relative to wild type controls (Fig. 2c,d; t-test, $p < 0.001$, $n = 18$). This result demonstrates that *tax-4* is required not only for chemotaxis in general, but also for klinotaxis in particular, thereby providing a new behavioral phenotype for this mutation.

Behavioral responses to temporal steps in osmolarity

C. elegans avoids a droplet of hyperosmotic fluid placed in its path by initiating a bout of reverse locomotion (Culotti and Russell, 1978; Hilliard et al., 2002). The main chemosensory neuron for detecting changes in osmolarity in *C. elegans* is ASH. This neuron is activated not only by sudden increases in osmolarity (on responses), but also by sudden decreases in osmolarity (off responses) (Chokshi et al., 2010). Whether osmotic avoidance is initiated by on responses, off responses, or both is unknown. This is because a freely moving worm immediately withdraws from an osmotic stimulus, thereby superimposing on and off responses.

To address this issue we used the device in its temporal operating mode. This was done by presenting two groups of worms with a temporal series of spatially symmetrical stimulus epochs. The series alternated between solutions of low and high osmotic strength (370 mOsm and 1000 mOsm, respectively) according to the counterbalanced design shown in Fig. 3a,b. As a control for possible mechanical artifacts of solution switching, a third group of animals was presented with mock solution changes between two reservoirs containing low osmolarity fluid (Fig. 3c).

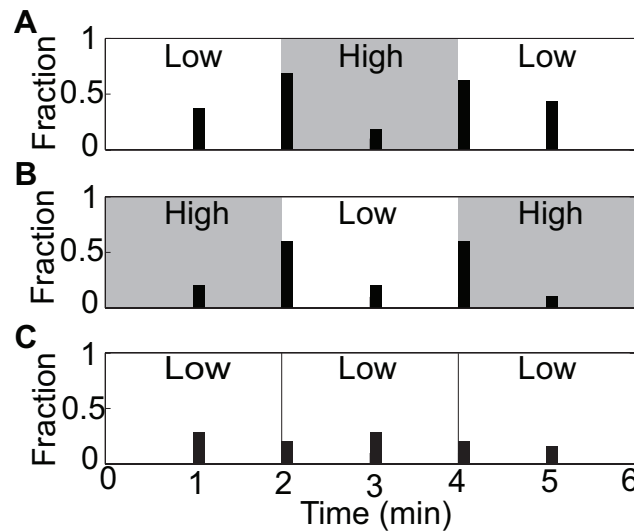


Figure 3. Behavioral responses to temporal steps in osmolarity. (a-c) Data are quantified as the fraction of worms that initiated at least one reversal in the 5 second interval beginning at the times shown on the abscissa. Shading indicates high osmolarity. Numbers of replications in a-c were 16, 10, and 25, respectively.

Behavior was quantified in terms of the fraction of worms that initiated at least one reversal in a 5 second interval at the beginning and the middle of each epoch. The switch from low to high osmotic strength caused an increase in reversal probability relative to controls (Fisher's exact test, $p < 0.0001$, $n = 51$), as did the switch from high to low osmotic strength (Fisher's exact test, $p < 0.001$, $n = 51$). Reversal probability was

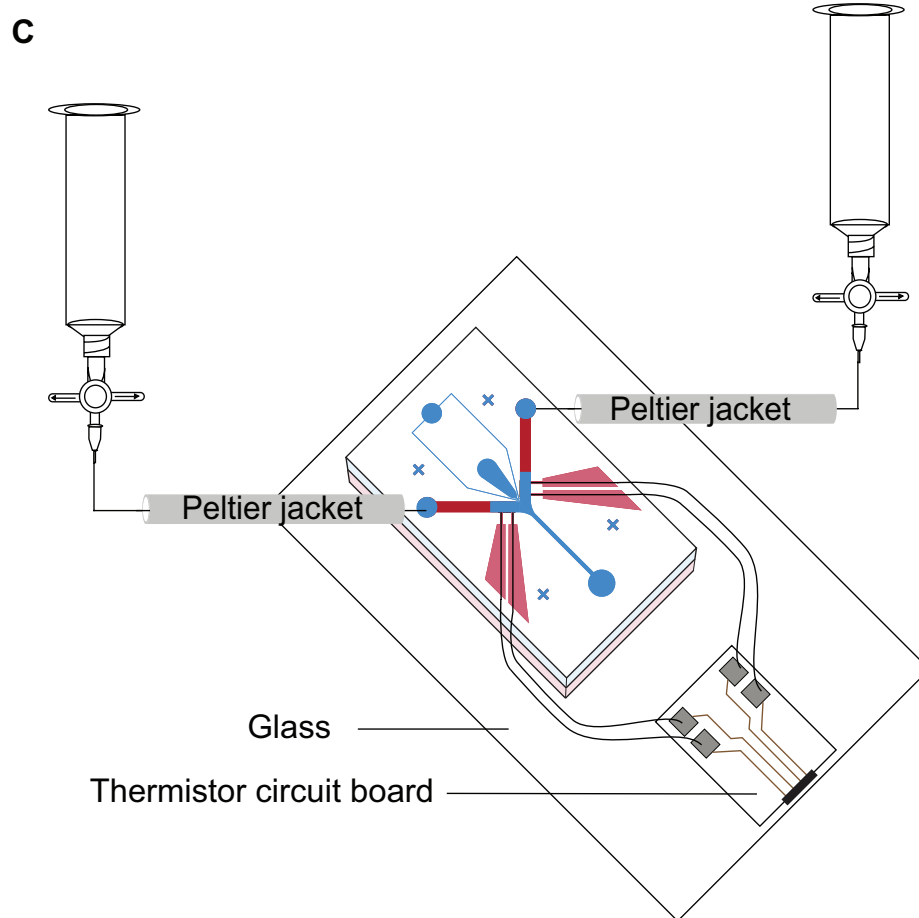
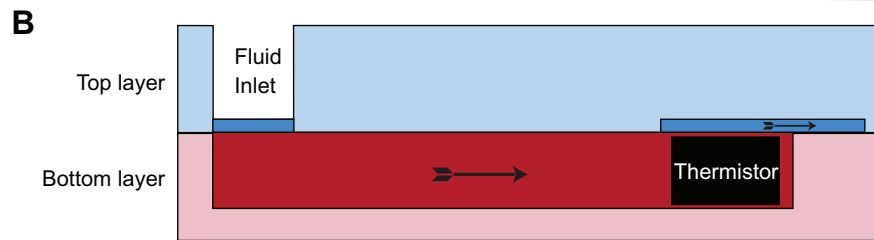
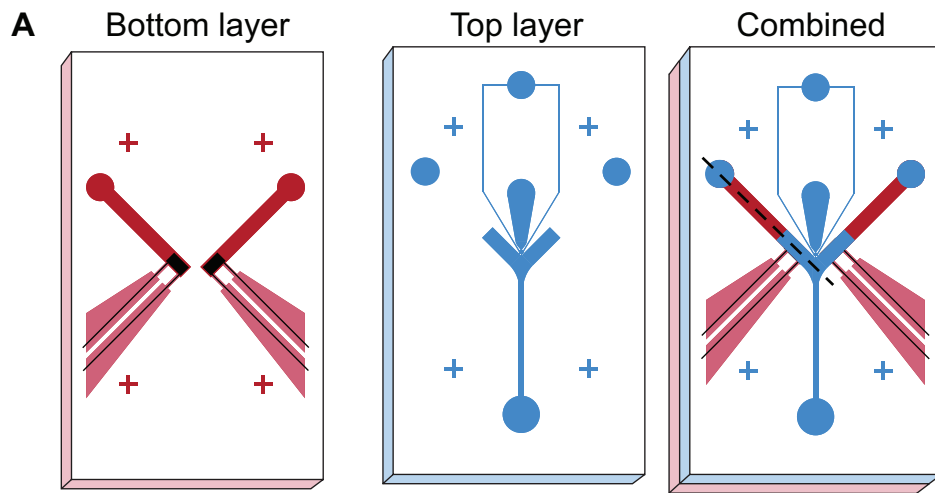
unaffected in the control group, indicating that reversal bouts were specifically the result of changes in osmolarity (Fisher's exact test, $p > 0.05$, $n = 25$). These results suggest that both on responses and off responses in ASH are sufficient to generate avoidance responses.

Design of the thermosensory device

The thermosensory device is designed to present the worm with a step-like thermal gradient. It is similar to the chemosensory device except that the arms of the Y-shaped channel are enlarged to accommodate a pair of thermistors located immediately upstream of the point of confluence. The thermistors are used to monitor the temperature of the two streams. This modification necessitated a two-layer design in which upper and lower PDMS layers are bonded with their feature sides apposed (Fig. 4a).

The upper layer contains the worm inlet, vacuum port and manifold, and the stem of the Y-shaped channel, including the point of confluence. The lower layer contains the arms of the Y-shaped channel with embedded thermistors and side channels for thermistor wires. Prior to assembly, the thermistors are fixed in place by filling the side

Figure 4 (next page). Design of the two-layer thermosensory device. (a) Top view showing the layout of channels in each layer before and after assembly (combined). The bottom layer (red) contains the arms of the device with embedded thermistors and wires (black). The top layer (blue) contains the worm restraint and the point of convergence of the fluid streams. (b) Side view through the plane indicated by dotted line in the combined view in (a). Saturated colors represent the channels through which fluid flows whereas less saturated colors represent bulk PDMS in each layer. Arrows indicate direction of flow. (c) Perspective view showing the arrangement of fluid reservoirs, Peltier tubing jackets for heating and cooling, and electrical contacts. Peltier jackets are controlled by an external temperature control module (not shown).



channels with optical adhesive which also seals these channels against fluid leaks. Fluid flowing in the lower layer reaches the upper layer by traveling up and over the thermistors (Fig. 4b). At the flow rates used in these experiments, we estimate that the travel time between thermistor and worm was less than 500 milliseconds. The temperature of the fluids entering each arm of the Y-shaped channel was manually regulated by separate Peltier devices (Fig. 4c). The thermosensory device was operated in spatial mode because of the length of time (30 seconds) required for temperature in the arms to equilibrate. After equilibration, temperature was stable to ± 0.5 °C for the duration of a typical experiment (~ 5 min).

Behavioral response to step gradients in temperature

To demonstrate the type of insights that can be gained with the thermosensory device, we investigated the behavioral mechanisms of thermotaxis. Thermotaxis in *C. elegans* involves klinokinesis (Ryu and Samuel, 2002; Zariwala et al., 2003), but whether klinotaxis also plays a role is unknown. To address this question, we cultivated worms under conditions known to make them prefer a temperature of 20 °C (Hedgecock and Russell, 1975) and exposed them in the device to fluid streams of 20 and 25 °C. Behavior was quantified in terms of average head angle (Fig. 1e) over a three minute trial such that positive angles corresponded to the head visiting the cooler stream. Temperature was randomized with respect to the left and right sides of the chip and the dorsoventral orientation of the worm. Under these conditions, head angle was clearly biased toward the 20 °C stream (Fig. 5; t-test, $p < 0.01$, $n = 16$). No such bias was observed in worms

exposed to streams of the same temperature (t-test, $p > 0.05$, $n = 19$ for the 15, 20, and 25 degree conditions), indicating that the effect was specific to the temperature difference. These findings are consistent with a role for klinotaxis during thermal migration in *C. elegans*, at least in steep thermal gradients. In a second experiment, worms cultivated at 20 °C but exposed to streams of 15 °C and 25 °C were biased toward the former (t-test, $p < 0.01$, $n = 19$). Thus, in a forced choice between two temperatures equidistant from the preferred temperature, worms appear to prefer the cooler temperature, consistent with the finding that in *C. elegans*, thermotaxis down a gradient is more robust than thermotaxis up a gradient (Ramot et al., 2008; Jurado et al., 2010; Ito et al., 2006).

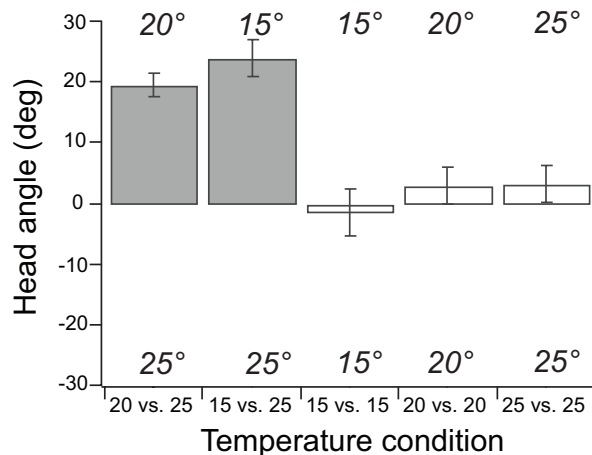


Figure 5. Behavioral response to step gradients in temperature. Mean head angle was computed as in Fig. 2d. Responses to five different temperature conditions are shown. Worms were cultivated at 20 °C. Shaded bars indicate asymmetrical temperatures. In each condition, the direction of the bar shows preferred temperature, if any. Error bars are s.e.m.

DISCUSSION

The device described here makes it possible to deliver spatial and temporal step gradients to semi-restrained *C. elegans*. A key feature of the device is a vacuum-assisted

restraint that aligns the long axis of the worm with the stable border between two solutions. As a result, the response of individual worms to multiple border crossings can be examined. Additionally, the clamp ensures that the worm always encounters the border at the same angle. Together, these two aspects of the device improve the statistical power of step response experiments relative to those that rely on incidental border crossings in freely moving worms (Albrecht and Bargmann, 2010; Wicks et al., 2000).

We used the device to investigate the spatial orientation strategies in *C. elegans* at the resolution of single head swings. By presenting spatial concentration steps of a chemoattractant, we were able to confirm the hypothesis that *C. elegans* can perform klinotaxis, at least in response to large concentration changes. However, our findings do not exclude the possibility that a different behavioral mechanism is utilized when concentration changes are small, nor do they necessarily imply that the same neuronal mechanism is involved. In analogous experiments using a thermal step, we found that *C. elegans* is also capable of using klinotaxis when navigating steep thermal gradients. Both types of experiment would have been difficult or perhaps impossible to interpret in the case of freely moving worms in continuous gradients where concentration, or temperature, changes throughout the head swing.

We also used the device to investigate responses to temporal steps in osmolarity. In these experiments we found that sudden changes in osmolarity trigger reversals not only when osmolarity rises but also when it falls. We hypothesize that the latter type of response was missed in previous studies of osmolarity responses because the unrestrained worm withdraws so quickly from the stimulus that on and off responses are

superimposed. This finding highlights the value of precise temporal control of stimulus presentation.

The device is readily adaptable to many other types of experiments. Orientation responses of wild type and mutant worms can now be studied at high resolution in response to spatial and temporal step gradients of a wide range of fluid borne cues including pH (Ward, 1973), odorants (Bargmann and Horvitz, 1991), pheromones (White et al., 2007), oxygen (Gray et al., 2004), carbon dioxide (Bretscher et al., 2011), and environmental toxins (Sambongi et al., 1999). Using the device in temporal mode, it should be possible to associate sensory cues with appetitive or aversive stimuli in simple classical conditioning experiments (Ardiel and Rankin, 2010). The effects of such treatments could then be tested by presenting the conditioned cues against each other in the device's spatial mode. With minor modifications, the device could be combined with on-line image processing to deliver spatial or temporal steps that are time-locked to particular behaviors or postures of the animal. Such experiments would make it possible to test dynamical models of sensorimotor integration in *C. elegans* (Izquierdo and Lockery, 2010). Finally, the transparency of the device makes it compatible with optogenetic approaches in which genetically targeted probes are used to record (Faumont and Lockery, 2006) and stimulate (Stirman et al., 2011; Leifer et al., 2011) individual neurons while the animal is moving. Such experiments are likely accelerate our understanding of the neuronal basis of behavior in this key model organism.

MATERIALS AND METHODS

Device fabrication

We fabricated both devices using standard soft lithographic methods (Qin et al., 2010). A silicon wafer master for the chemosensory device was created by exposing a 60 μm layer of SU-8 2025 resist (Microchem, Newton, MA) through a transparency mask and dissolving away unexposed material. Masters for the top and bottom layers of the thermosensory device were created by exposing 60 and 500 μm layers of SU-8 2025 and SU-8 2075, respectively. Masters were treated with chlorotrimethylsilane (Aldrich, St. Louis, MO) to prevent adhesion of PDMS to the master. Masters were replica molded in PDMS (Dow Corning Sylgard 184, Corning, NY). Holes for ports and inlets (1.0 or 1.5 mm diam.) were formed using a biopsy punch. Thermistors (Panasonic NTC JZ(0201)) and associated wires were embedded into channels in the lower layer of the thermosensory device with UV-sensitive optical glue (Norland 81, Norland, Cranbury, NJ). PDMS castings were bonded to their respective substrates after 30 sec exposure to an oxidizing air plasma. To facilitate alignment in two layer devices, castings were moistened with methanol immediately prior to assembly. As the methanol evaporated, the feature sides came into contact and bonded tightly. The device assembled device was then placed in a polycarbonate clamp and thermistor wires were soldered to an external circuit board.

***C. elegans* cultivation**

Synchronous populations of wild type (N2) and mutant (*tax-4(p678)*) *C. elegans* were grown on standard nematode growth medium (NGM) plates seeded with *E. coli* OP50 as described (Stiernagle, 2006). On the first day of adulthood, worms were picked to an unseeded NGM plate and allowed to crawl free of any co-transported food. Worms used in chemosensory and osmosensory experiments were starved for 30-60 minutes prior to experiments whereas worms used in thermosensory experiments were maintained in food until use.

Solutions

In chemosensory experiments, the solutions contained (in mM) 1 CaCl₂, 1 MgSO₄, 10 HEPES, and NaCl as indicated in the text. Glycerol was added to achieve a total osmolarity of 370 mOsm. Similar solutions were used in osmolarity experiments except that the concentration of NaCl was 1 μM and osmolarity was adjusted to 370 mOsm or 1000 mOsm in the low and high osmolarity solutions, respectively. In thermosensory experiments, the solution used was S Basal (Stiernagle, 2006). All solutions were filtered with a pore size of 0.22 μm prior to use. In thermosensory experiments, temperature was regulated by a peltier temperature control system (TC2BIP with CH module, Cell MicroControls, Norfolk, VA). Flow rates through the device were 10-15 mL per hour.

Data collection and analysis

Video recordings of worm behavior (30 frames/sec) were analyzed in MATLAB using a custom routine to compute head angle θ in each image. Briefly, frames were first masked and thresholded to obtain an image of the worm. The centerline of the worm was then obtained by a skeletonization procedure. Starting at the position of the clamp, the centerline was traversed to find the tip of the head, defined as the point furthest from the clamp. Initiation of reversals was scored manually by an observer who was blind to experimental condition. Reversal behavior was defined as propagation of the undulatory wave in the posterior to anterior direction as previously described (Faumont et al, 2005).

BRIDGE

In this chapter, we described in detail the microfluidic device known as the Y-chip. This microfluidic device is used extensively throughout the remainder of this dissertation to analyze the behavioral aspects of klinotaxis behavior in *C. elegans* and examine its neuronal basis.

CHAPTER III

LEFT / RIGHT ASYMMETRY IN THE NEURAL NETWORK UNDERLYING KLINOTAXIS IN *CAENORHABDITIS ELEGANS*

A final account of this chapter will be submitted for publication with Dr. Shawn Lockery as a co-author. Dr. Lockery assisted with experimental design.

INTRODUCTION

The roundworm *Caenorhabditis elegans* lives in decomposing vegetal matter, and crawls on its side, undulating in the dorsal-ventral plane. *C. elegans* orients to gradients of attractive chemical stimuli, e.g. sodium chloride, using two main strategies (Faumont et al., 2012). The first strategy is a biased random walk, which is known in the *C. elegans* literature as the pirouette strategy (Pierce-Shimomura et al., 1999), but is more generally termed klinokinesis (Fraenkel and Gunn, 1940). In this strategy, the concentration of a chemoattractant is compared over time such that when the derivative is positive, the animal continues going forward and, conversely, when the derivative is negative, the animal initiates a reversal and changes heading (Suzuki et al., 2008). Over time, this strategy results in navigation to peaks of attractive chemicals. The second strategy, known in the *C. elegans* literature as the weathervane strategy but more generally termed

klinotaxis, is less well studied. In this strategy, animals bias their forward-going locomotion such that the path taken curves gradually to ascend a chemical gradient (Iino and Yoshida, 2009).

Klinotaxis is a directed response to a gradient whereas klinokinesis is undirected, hence klinotaxis is more efficient (Fraenkel and Gunn, 1940; Dunn, 1990). Behavioral responses involved in klinotaxis depend on the internal state of the animal in a way that those in klinokinesis do not. In klinokinesis, a decrease in concentration can only result in a reversal whereas, in klinotaxis, the same decrease in concentration must be paired with the body posture of the animal to produce an appropriate response (Faumont et al., 2012). If the concentration of the attractive stimulus is lower on the worm's dorsal side, the worm must curve ventrally to ascend the gradient. Conversely, if the concentration of the attractive stimulus is lower on the worm's ventral side, the worm must curve dorsally to ascend the gradient.

The ASE class of sensory neurons and the AIZ class of interneurons have been implicated in both klinotaxis and klinokinesis (Iino and Yoshida, 2009; Suzuki et al., 2008). Although they share neurons, the downstream processing in the neuronal circuits that give rise to klinotaxis and klinokinesis are likely to differ substantially. Because klinotaxis has more contextual dependencies than klinokinesis, the architecture of the network underlying klinotaxis is expected to be more complex. So far, no motor neuron class has been identified to play a role in klinotaxis. The ASE neurons are known to have a left / right functional asymmetry, with the ASEL neuron responding to increases in salt

(ON cell), and the ASER neuron responding to decreases in salt (OFF cell). Whether and how the differing responses ASE neurons function to underlie klinotaxis is unknown.

Here I present a characterization of klinotaxis using a sophisticated microfluidic device that splits the sensory environment encountered by the worm across the head sweep in two (McCormick et al., 2011). Because klinotaxis involves a comparison in sensory environment across the head sweep, this device allows us to provide a consistent stimulus for klinotaxis. Using this device, I explored a putative minimal neural network that I hypothesized to underlie klinotaxis and found evidence that this network was necessary for normal klinotaxis. Further behavioral analysis revealed distinct functions for the left and right neurons in this network. This work suggests that information in the network underlying klinotaxis is segregated into left and right streams. Hence, left/right differentiation could be an important feature of circuits that underlie behavior in this simple metazoan.

RESULTS

Behavioral mechanisms of klinotaxis

A key characteristic of klinotaxis is that the intensity of a stimulus is compared between lateral sampling points of the sensory organ. In order to confirm that worms are using this information to orient, I used a microfluidic device that takes advantage of laminar flow such that the sensory environment encountered by the worm across the head sweep is split in two (McCormick et al., 2011). When the two environments are composed of the same solution, locomotion is relatively balanced between dorsal and

ventral excursions. However, when one environment is composed of a higher concentration of chemoattractant than the other (in this study, 50mM vs. 0mM NaCl), the worm biases its locomotion toward the high-concentration side (Figure 1A).

The fundamental unit of forward locomotion in *C. elegans* is a single dorsoventral undulation cycle, repeated in time to generate thrust. This unit also provides the lateral sampling points that are needed for klinotaxis. Thus, we decided to analyze aspects of individual cycles to understand how locomotion becomes biased (Figure 1B). The bias is expressed in several ways. The peak amplitude of the portion of the undulation cycle in the high concentration region is increased ($t(56) = 6.35, p < 0.001$), whereas the peak amplitude of the portion of the undulation cycle in the low concentration region is reduced ($t(56) = 13.53, p < 0.001$; e.g. Figure 1C). Similarly, the duration of the portion of the undulation cycle in the high concentration region is increased ($t(56) = 7.01, p < 0.001$), whereas the duration of the portion of the undulation cycle in the low concentration region is reduced ($t(56) = 8.03, p < 0.001$; e.g. Figure 1D). The totality of the data is best summarized through a measure that combines these properties into an integral. The integral of the portion of the undulation cycle in the high concentration region is increased ($t(56) = 7.24, p < 0.001$), whereas the integral of the portion of the undulation cycle in the low concentration region is reduced ($t(56) = 4.73, p < 0.001$; e.g. Figure 1E). To generate a representation of the average undulation cycle, I normalized the time component of the cycles into phase (Figure 1F). This analysis provides a visual way to compare data, and allows the reader to assess modulations of the duty cycle.

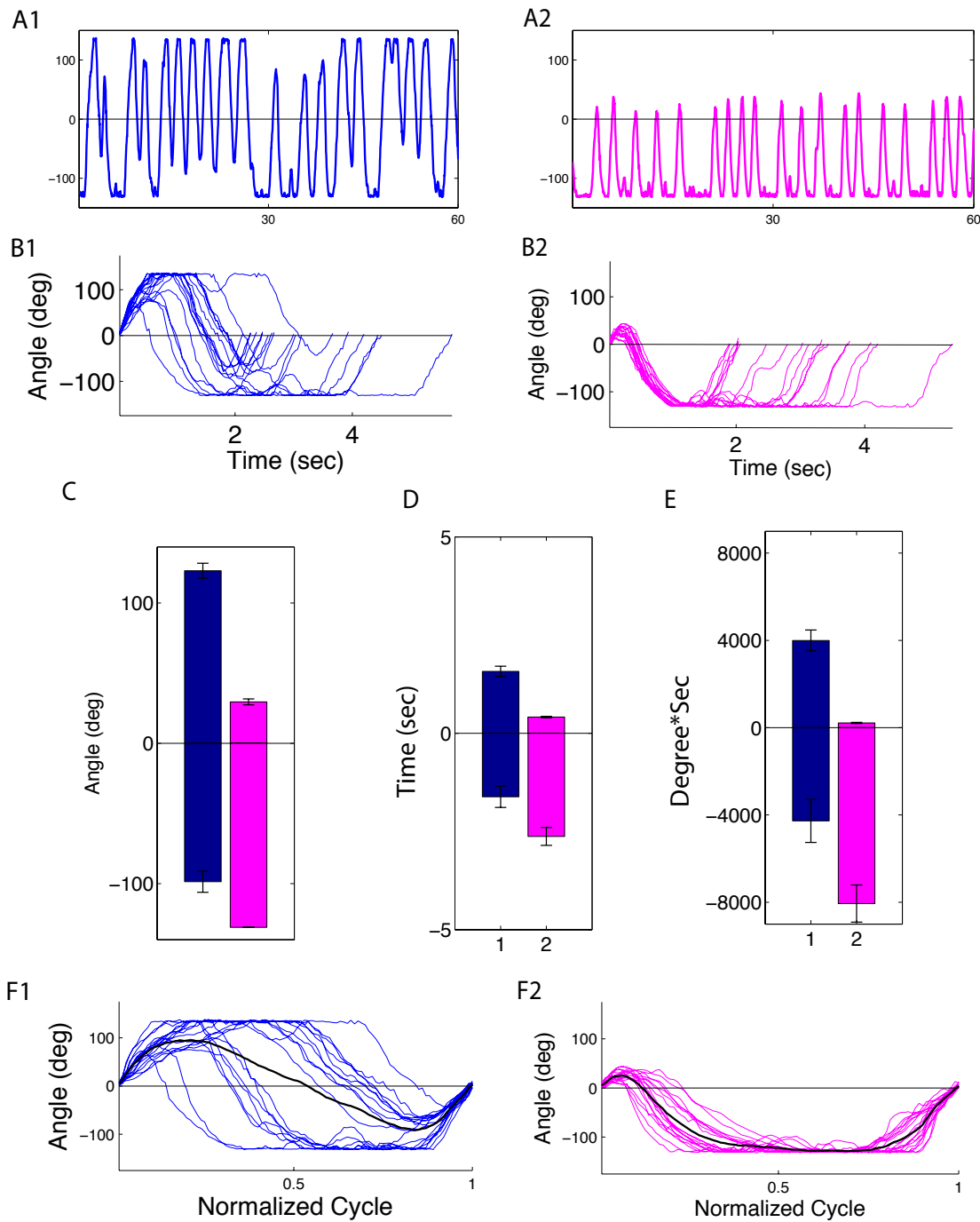


Figure 1. Analysis of klinotaxis behavior in an individual N2 worm. (A1) Example of behavior in symmetrical solutions, 0.001 mM NaCl. (A2) The same worm's behavior when 50 mM NaCl is placed in the negative head angle region. (B1, B2) Individual cycles from the above traces. (C) Mean peak amplitude for the locomotion cycles in (B1, B2). (D) Mean duration of the locomotion cycles in (B1, B2). (E) Mean integral of the locomotion cycles in (B1, B2). (F1, F2) Normalized cycles in (B1, B2). Bold black traces are the mean of the individual traces. Error bars are S.E.M.

Bias increases as a function of concentration difference

I tested worms' ability to klinotax to four levels of concentration difference: 0mM, 1mM, 10mM and 50mM. The mean angle of the head during the test epoch, a measure of the degree of bias during klinotaxis, was strongly influenced by the test concentration difference ($F(3,154) = 71.7$, $p < 0.001$, 0mM: Mean = 3.62 degrees, 1mM: Mean = -10.53 degrees, 10mM: Mean = -47.36 degrees, 50mM: Mean = -64.17 degrees). The integral for both the portion of the cycle in low salt ($F(3,154) = 32.59$, $p < 0.001$) and the portion of the cycles in high salt ($F(3,154) = 90.11$, $p < 0.001$) were also significantly affected (Figure 2). Comparing 0mM vs. 1mM concentration difference, the integral of the portion of the undulation cycle in the low concentration region was reduced ($t(64) = 2.12$, $p = 0.037$), whereas the integral of the portion of the undulation cycle on the high concentration side was unaffected ($t(64) = 1.47$, $p = 0.14$, Figure 2C). The bias to locomotion increased with concentration difference (Figure 2A, B), such that worms tested at a 10mM difference decreased the integral of the portion of the undulation cycle in the low concentration ($t(48) = 3.70$, $p < 0.001$) and increased the integral of the portion of the undulation cycle in the high concentration ($t(48) = 5.28$, $p < 0.001$) relative to those tested at 1mM. Worms tested at 50mM concentration difference increased the integral of the portion of the undulation cycle in the high concentration relative to those tested at 10mM ($t(44) = 3.29$, $p = 0.002$), whereas the integral of the portion of the undulation cycle in the low concentration was not further reduced ($t(44) = 0.09$, $p = 0.92$). Scaling of the bias to locomotion with concentration difference could be an

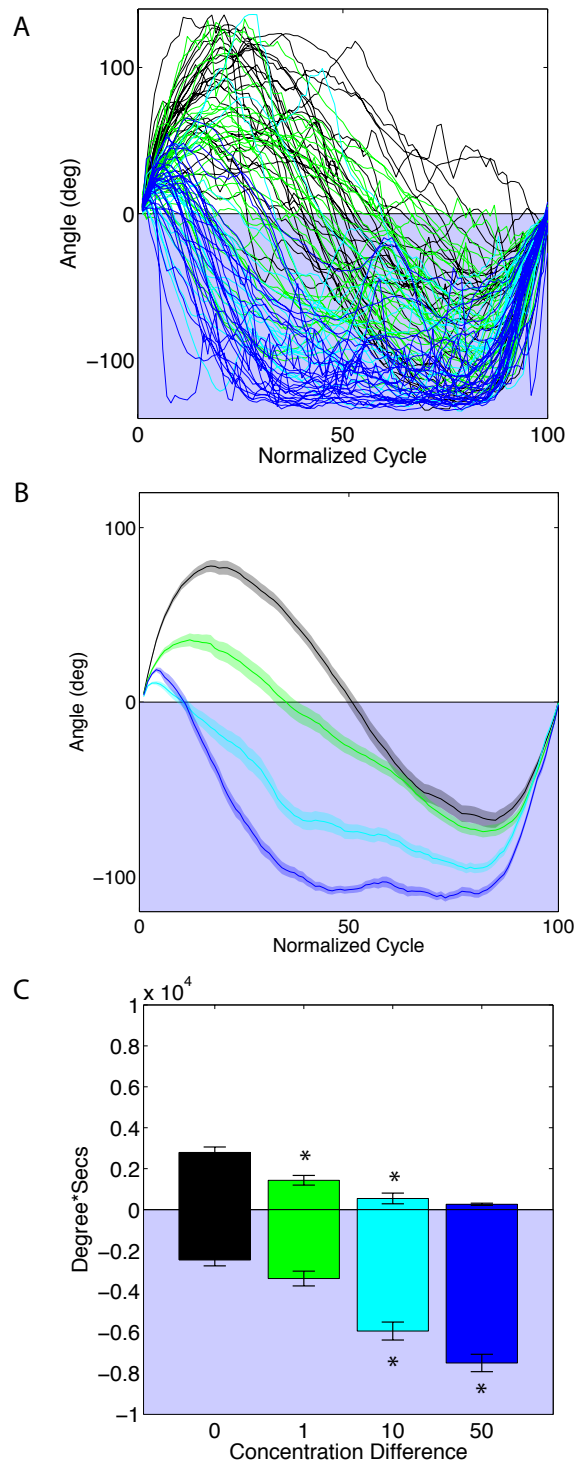


Figure 2. Klinotaxis bias scales with concentration difference. (A) Average normalized cycles for all worms tested. Black, no concentration difference. Green, 1mM concentration difference. Cyan, 10mM concentration difference. Blue, 50mM concentration difference. (B) Mean of the averaged normalized cycles. (C) Mean integral of the individual cycles in time. Error bars and transparent regions are S.E.M.

important feature of klinotaxis because it enables worms that are crawling obliquely up a gradient to course-correct towards a more direct angle of ascent.

Hypothesized neural circuitry

Identifying a Putative Minimal Network. Understanding the neural circuitry underlying klinotaxis first requires identification of a set of neurons that are well situated, both in their physical structure and their known properties, to transform the sensory input that triggers the behavior into the motor command that enacts it. I first identified a putative minimal network, composed of the smallest possible set of neurons that could take transform the internal neuronal signal from sensory inputs to motor outputs. To generate this putative neural circuit, I integrated the detailed wiring diagram data on the *C. elegans* nervous system (White et al., 1986) with neuronal data from prior studies. The wiring diagram was generated through serial thin-slice reconstruction and provides data on the number of synaptic contacts between any two neurons.

A previous study identified the ASE and AIZ neurons as having large effects on klinotaxis when ablated (Iino and Yoshida, 2009), so I confined my search to networks that included these two neurons. ASE does not innervate AIZ directly, but must go through a minimum of one other interneuron. I identified AIY as the key first-layer interneuron in our minimal network by optimizing for both shortest path length and most synaptic contacts. I next searched for a motor neuron class that had synaptic contacts with the interneuron AIZ, and with both the dorsal and ventral muscles of the head, as required for klinotaxis. The SMB motor neurons are densely innervated by the AIZ

neurons, receiving more synaptic contacts from AIZ than any other neuron class and receiving more than three times as many synaptic contacts as any other motor neuron (White et al., 1986). The SMBs also have synaptic contacts with the dorsal and ventral head muscles (muscles 1-8) of *C. elegans* in roughly equal number (White et al., 1986). Additionally, ablation of SMBs is noted to cause loopy, high-amplitude locomotion (Gray et al., 2005). As previously shown, the amplitude of locomotion is modulated in klinotaxis (Figure 1). Hence, I hypothesized the SMB class as key motor neurons in the minimal klinotaxis network (Figure 3). This network was identical to the minimal network identified by Izquierdo and Beer (2013) through analysis of wiring diagram data alone. Hence, this putative minimal network is a strongly supported hypothesis circuit to instantiate the sensorimotor transformation underlying klinotaxis.

Laterality of Putative Minimal Network. Because the ASE left and right cells have opposing calcium concentration changes in response to the addition and subtraction of salt stimuli (Suzuki et al., 2008), we decided to look at the downstream connectivity of left and right cells individually. We noted that these cells made many more synaptic contacts with the ipsilateral member of candidate downstream interneurons than with contralateral members (White et al., 1986; Chen et al. 2006). To quantify this finding, we defined a laterality index that ranges from -1 to 1, in which an index of 1 indicates that only ipsilateral synaptic contacts are present, -1 indicates that only contralateral synaptic contacts are present, and an index of 0 indicates an equal number of ipsi- and contralateral synaptic contacts (see Materials and Methods). The projections of ASEL to the AIY interneuron layer had a laterality index of 0.68, and the projections of ASER to

the AIY interneuron layer had a laterality index of 0.77, indicating that the synaptic contacts of the sensory cells onto the first-layer interneurons were strongly ipsilateral. The AIY interneurons synapsed only with ipsilateral AIZ interneurons, giving each a laterality index of 1.0. The same was true for synaptic contacts between AIZ's and SMB's. Although the strong laterality of these synaptic projections is probably somewhat mitigated by gap junctions between the left and right members within the AIY and AIZ interneuron classes (1 and 2 gap junctions, respectively), this strong, circuit wide ipsilateral bias in synaptic contacts motivated us to assess the contributions of left and right members of candidate neurons in the klinotaxis circuit separately.

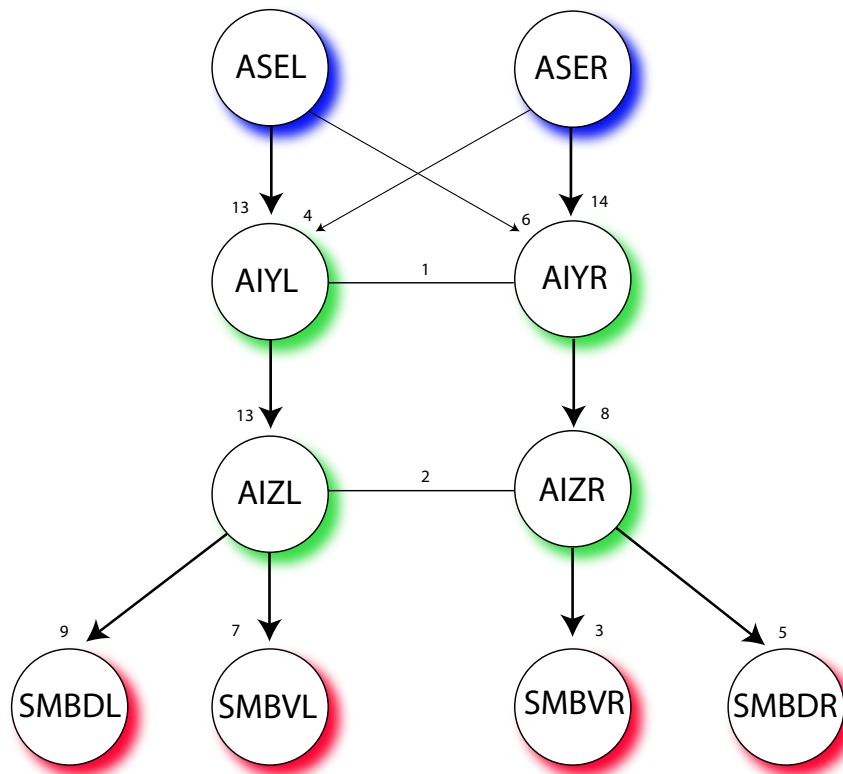


Figure 3. Minimal neural network underlying klinotaxis. Blue shadow, sensory neurons. Green shadow, interneurons. Red shadow, motoneurons. Arrows represent synaptic contacts, connective lines represent electrical junctions. Numbers represent the number of contacts (White et al., 1986).

Ablation and genetic manipulation of proposed neural circuitry

Sensory Neurons. The left and right members of the ASE neuron class are known to have different but complementary preferred stimuli (Suzuki et al., 2008). ASEL responds to sustained stepwise increases in salt concentration with increased calcium signal (ON cell), whereas ASER responds to sustained stepwise decreases in salt concentration with an increased calcium signal (OFF cell). Contrary to the results of prior studies (Iino and Yoshida, 2009), we found that ablating ASEL alone led to significant impairment of normal klinotaxis. Ablation led to significant effects both on the portion of the locomotion cycle that followed a stepwise increase in salt (ON stimulus; Figure 4 A1, peak amplitude, $t(25) = 3.53$, $p = 0.002$; integral: $t(25) = 2.12$, $p = 0.04$), and on the portion of the cycle that followed a stepwise decrease in salt (OFF stimulus; Figure 4 A1, peak amplitude: $t(25) = 3.11$, $p = 0.005$; B1: duration, $t(25) = 2.14$, $p = 0.04$; C1: integral, $t(25) = 1.92$, $p = 0.01$).

We found that ablation of ASER (OFF cell) led to significant changes only to the portion of the cycle that followed a decrease in salt (OFF stimulus). Ablated animals increased the peak amplitude of the excursion into the low-concentration region of the sensory environment (Figure 4 A2, $t(24) = 4.44$, $p < 0.001$) and increased the amount of time spent there (Figure 4 B2, $t(24) = 2.75$, $p = 0.01$) relative to mock ablated controls. There was a concomitant increase in the integral of the path taken in the low-concentration region of the device (Figure 4 C2, $t(24) = 2.92$, $p = 0.008$).

These findings suggest that the ASE neurons respond on the time scale of individual locomotory cycles to track changes in the concentration of chemoattractant encountered

during a head swing. The ASER (OFF) cell supports appropriate behavioral responses during the portion of the phase that follows its preferred stimulus (OFF stimulus), whereas the ASEL (ON) cell supports appropriate behavioral responses during the portions of the phase following both the ON and the OFF stimulus.

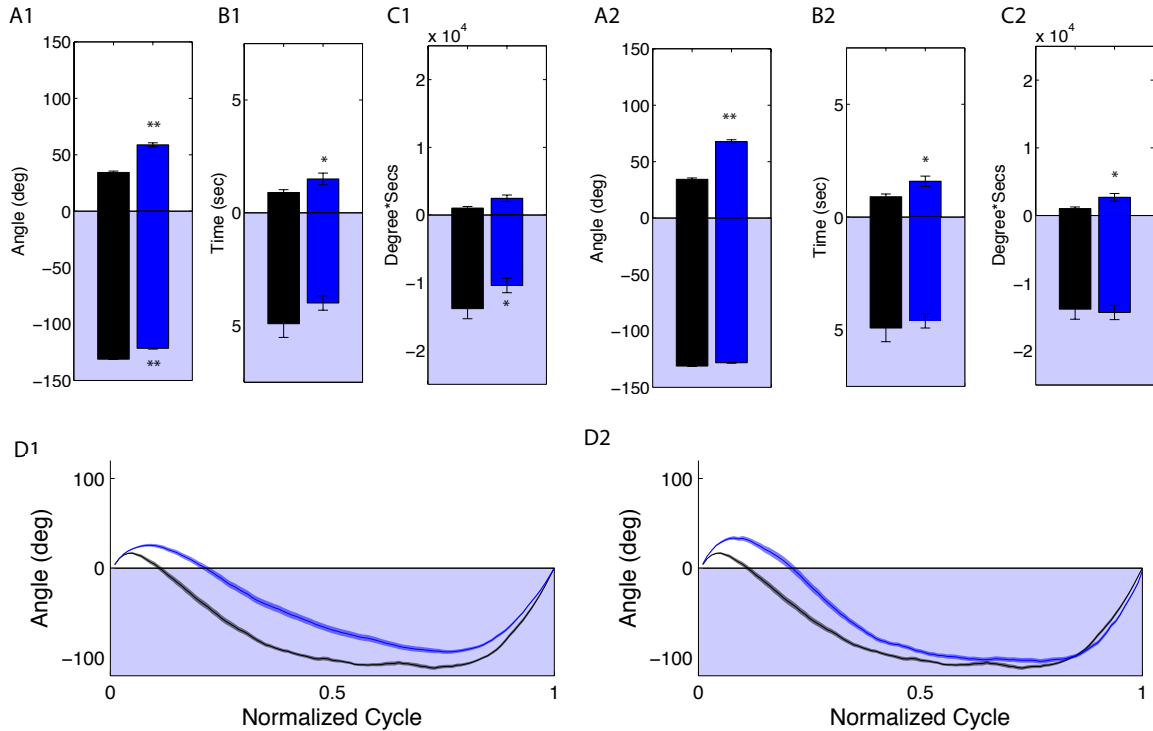


Figure 4. Effects of Ablation of ASE neurons. Column 1, ASEL ablated in blue (n=13), sham ablated in black (n=14). Column 2, ASER ablated in blue (n=12), sham ablated in black (n=14). (A) Mean peak amplitude. (B) Mean duration. (C). Mean integral. Light blue shaded region indicates the presence of high-concentration NaCl (50mM). (D) Normalized cycles. Error bars and transparent regions represent S.E.M. * = p < 0.05, ** = p < 0.005.

Interneurons. Ablation of the AIY neurons had no effect on klinotaxis in our study, similar to the results of klinotaxis studies performed on agar plates (Iino and Yoshida, 2009), (Figure 5, peak amplitude following OFF stimulus: $t(30) = 1.25, p = 0.22$; peak amplitude following ON stimulus: $t(30) = 0.65, p = 0.51$). This could be because of

developmental accommodation or neurites that persist in the absence of the cell body. However, mutants of *ttx-3* (*OH161*), a LIM homeodomain protein that expresses strongly and consistently in AIY neurons and is required for other functions of AIY (Altun-Gultekin et al., 2001; Remy and Hobert, 2005), were impaired in their ability to do klinotaxis (Figure 5, peak amplitude following OFF stimulus: $t(54) = 8.13, p < 0.001$). Another *ttx-3* mutant, OH8, had a bimodal distribution on klinotaxis indices, but was not significantly different from control on average (peak amplitude following OFF stimulus: $t(38) = 0.73, p = 0.46$, peak amplitude following ON stimulus: $t(38) = 0.58, p = 0.56$). Because ablation had no effects and there is currently no cell-specific promoter for the AIY class, we were unable to assess the contributions of the AIYR and AIYL cells independently.

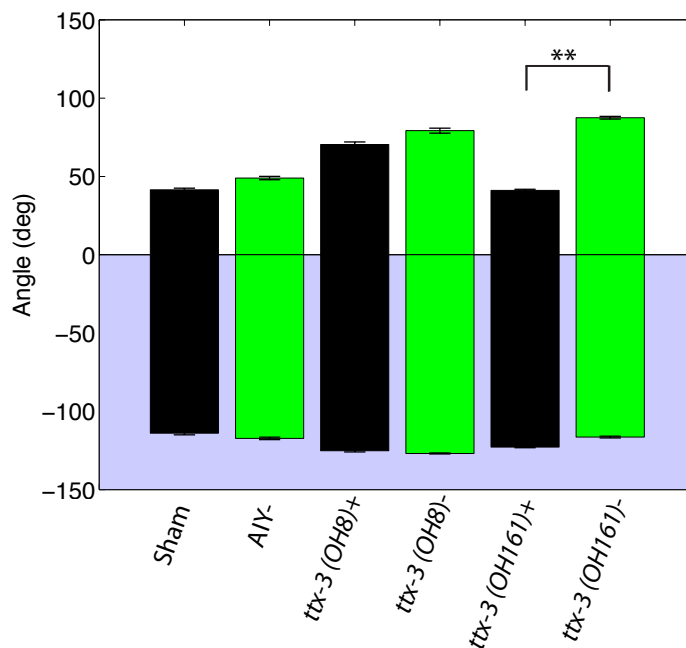


Figure 5. Effects of ablation and genetic manipulation of AIY neurons on mean peak amplitude. Sham AIY ablated, n = 14; AIY ablated n = 18; *ttx-3*(OH8) parallel controls n = 14; *ttx-3*(OH8) n = 26; *ttx-3*(OH161) parallel controls, n = 29; *ttx-3*(OH161), n = 27.

Ablation of the AIZL neuron had no statistically significant effects; however, the changes in mean duration and integral of the high-concentration portion of the undulation cycle, following a ON stimulus, were in the same direction as the changes induced by ablation of ASEL (Figure 6 A1, B1, C1, D1). Ablation of the AIZR neuron caused significant changes only to the low-concentration portion of the locomotion cycle following an OFF stimulus. The peak amplitude of the low-concentration excursion was increased (Figure 6 A2, $t(26) = 3.40$, $p = 0.003$) as was the duration (Figure 6 B2, $t(26) = 3.03$, $p = 0.006$) and the integral (Figure 6 C2, $t(26) = 2.99$, $p = 0.006$). These results demonstrate that the AIZL and AIZR neurons have different effects on the worms' ability to do klinotaxis. AIZR ablation had consistent effects on low-concentration portion of the cycle following an OFF stimulus, echoing the effects of ablation of ASER.

Motor Neurons

The SMB neuron class has a fourfold symmetry such that there are dorsal and ventral members on both the left and right sides (White et al., 1986; Figure 3). We ablated the left and right members of the SMB neuron class separately to assess the whether the distinct functions observed in upper layers of the network propagated to this motor neuron layer. We found that ablation of SMBLs led to small but significant changes of the peak amplitude on both the high-concentration ($t(26) = 2.18$, $p = 0.04$) and low-concentration portions of the locomotion cycle (Figure 7 A1, $t(26) = 2.57$, $p = 0.02$), whereas ablation of SMBRs had effects only on the peak amplitude of the low-concentration excursion following a OFF stimulus (Figure 7 A2, $t(16) = 3.54$, $p = 0.003$).

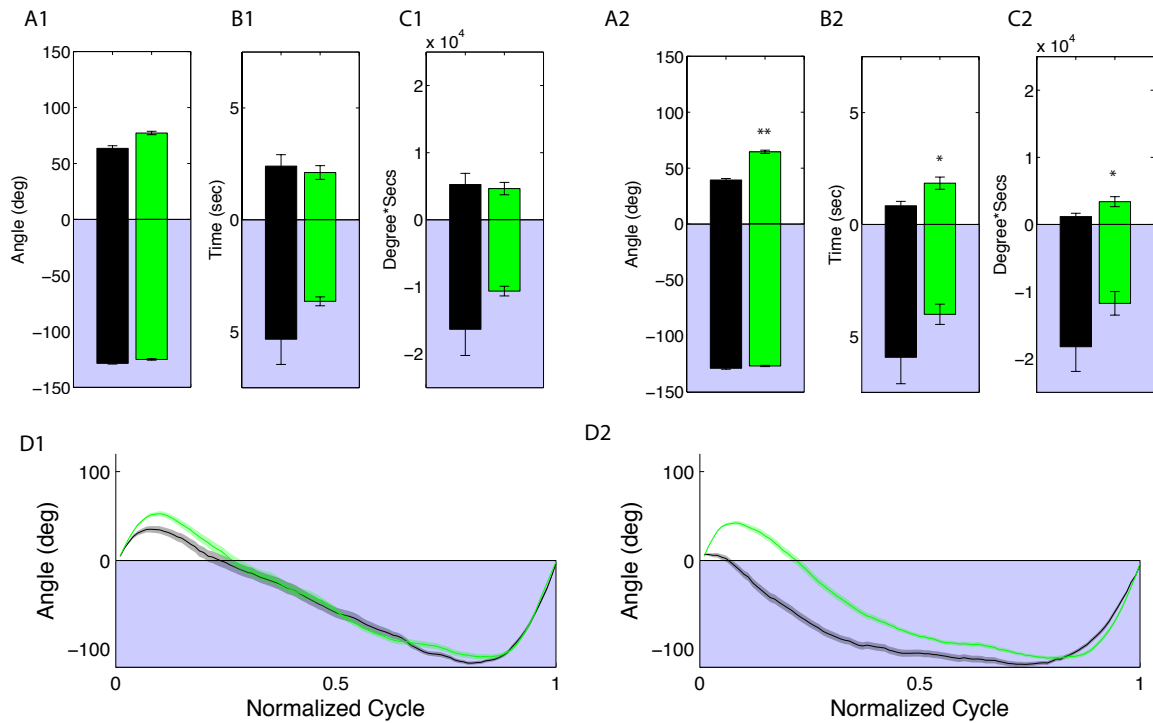


Figure 6. Effects of Ablation of AIZ neurons. Column 1, AIZL ablated in blue (n=11), sham ablated in black (n=14). Column 2, AIZR ablated in blue (n=13), sham ablated in black (n=15). (A) Mean peak amplitude. (B) Mean duration. (C). Mean integral. Light blue shaded region indicates the presence of high-concentration NaCl (50mM). (D) Normalized cycles. Error bars and transparent regions represent S.E.M. * = $p < 0.05$, ** = $p < 0.005$.

The mean integral of the high-concentration portion of the cycle was increased for SMB DR/VR ablated animals (Figure 7 C2, $t(16) = 3.40$, $p = 0.004$). The mean integral of the low-concentration portion of the cycles was decreased for SMB DL/VL ablated animals ($t(26) = 2.11$, $p = 0.04$). When SMBDR/VR was ablated, the duration of time spent per cycle in both the low-concentration ($t(16) = 2.58$, $p = 0.02$) and the high-concentration region ($t(16) = 2.99$, $p = 0.009$) were increased. These results demonstrate that the SMBLs and SMBRs have different functions in creating normal klinotaxis. The SMBRs are necessary for normal amplitude on the portion of the locomotion cycle that follows a decrease in concentration (OFF stimulus), similar to AIZR and ASER. Ablation

of SMBRs but make the animals locomote more slowly and with higher curvature and higher amplitude at baseline (see Chapter IV). The SMBLs have smaller effects that are distributed between both portions of the locomotion cycle.

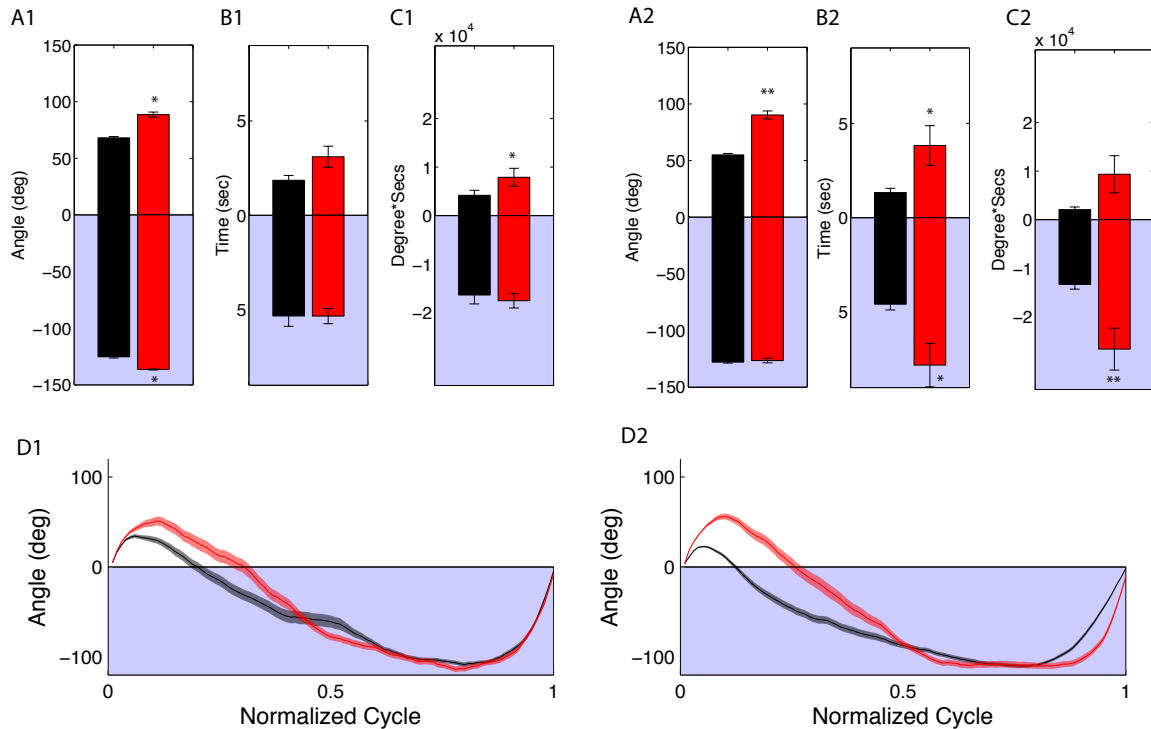


Figure 7. Effects of Ablation of SMB neurons. Column 1, SMB dorsal and ventral left (DL/VL) ablated in blue (n=14), sham ablated in black (n=14). Column 2, SMB dorsal and ventral right (DR/VR) ablated in blue (n=8), sham ablated in black (n=10). (A) Mean peak amplitude. (B) Mean duration. (C). Mean integral. Light blue shaded region indicates the presence of high-concentration NaCl (50mM). (D) Normalized cycles. Error bars and transparent regions represent S.E.M. * = $p < 0.05$, ** = $p < 0.005$.

DISCUSSION

In this study, we corroborate the claim that *C. elegans* uses klinotaxis as a spatial orientation strategy by testing worms in a specialized microfluidic device that splits the

sensory environment encountered by the worm across the head sweep in two (McCormick et al., 2011). This device allows us to conclude that the worm compares stimulus intensity at lateral sampling points of the head sweep and biases forward locomotion toward the preferred stimulus. This is an important mechanistic linkage to studies of klinotaxis in other organisms, such as larvae of the species *Drosophila melanogaster*, who actively sample the environment with lateral head casting to determine the direction of turns (Gomez-Marin et al., 2011).

Additionally, we provide evidence that the mechanisms underlying the bias in locomotion to a preferred side involve modulations of the peak amplitude, duration, and integral of the excursions to both the preferred and non-preferred sides. We also show that bias increases as a function of concentration difference between two lateral sampling points. The monotonically increasing function linking degree of concentration difference with degree of bias provides a possible mechanism for the animal to determine a more direct path up a salt gradient in the case that the animal is moving up it obliquely.

We propose and investigate a putative minimal network for klinotaxis, supported by both the *C. elegans* wiring diagram data and by prior behavioral studies. We find evidence that all neuron classes in the putative minimal network are required for klinotaxis, although no ablation completely abolished the behavior. This finding suggests the presence of alternative neurons and redundant processing pathways. We note, however, that the stimulus used to elicit klinotaxis in this study (50mM concentration difference) is much stronger than the stimulus used in a prior agar plate study (calculated 0.1mM concentration difference, Iino and Yoshida, 2009), or what is likely encountered

in natural settings. Our inability to completely abolish klinotaxis behavior through ablation of a single neuron or neuron class may be a reflection on the strength of the stimulus rather than evidence against the importance of the network investigated here.

We also present evidence that the putative neuronal network underlying klinotaxis behavior in *C. elegans* displays left-right asymmetry or lateralization. This asymmetry is evidenced in the strongly ipsilateral projections of the neurons of the network from one layer to the next (White et al., 1986; Chen et al. 2006). Ablation of the left and right members of the neurons implicated in the network revealed that while effects can be mixed, the left-sided neurons alone function to support normal peak amplitudes for klinotaxis on the portion of the locomotion cycle preceded by an increase in chemoattractant, the preferred stimulus of the ON-cell ASEL, whereas the right sided neurons predominantly function to support normal klinotaxis on the portion of the locomotion cycle preceded by a decrease in chemoattractant, the preferred stimulus of the OFF-cell ASER. This is the first work, to our knowledge, that assess the contribution of the left and right neurons in a sensorimotor network underlying a defined behavior.

Left/right asymmetries are known to be important in neural structure and behavior of all vertebrate taxa and for insects such as flies, ants, and bees. In humans and non-human primates, the left hemisphere is dominant in perceiving and expressing intentional communications such as language whereas the right hemisphere is dominant in perceiving and expressing emotional communications (Lindell, 2013). In other vertebrates, the left hemisphere dominates in quotidian activities such as feeding whereas the right hemisphere dominates in acute emotional challenges such as encounters with

predators (Vallortigara and Rogers, 2005). It is hypothesized that lateralization serves the purpose of increasing neural capacity by reducing redundancies (Vallortigara and Rogers, 2005). In *C. elegans*, lateral asymmetries at the cellular and sub-cellular levels have been studied for some time (Taylor et al., 2010; Chang et al., 2003; Suzuki et al., 2008). However, circuit level analysis that distinguishes between the left and right halves of the nervous system is almost completely absent in the *C. elegans* literature.

Lateralization of brain function is emerging as a common feature of metazoan nervous systems (Oklenburg and Güntürkün, 2012). It is hypothesized that lateralization serves the purpose of increasing neural capacity by reducing redundancies (Vallortigara and Rogers, 2005). The worm as a model organism offers distinct advantages for studying hypotheses about lateralization, including a compact nervous system, a complete wiring diagram of synaptic contacts, and genetic tractability. Further studies of the laterality of the neural circuits that underlie behavior in *C. elegans* could provide insight into a highly conserved neural attribute.

MATERIALS AND METHODS

Cultivation and strains

C. elegans were grown at 20° C on standard nematode growth medium (NGM) plates seeded with *E. coli* OP50 as described (Stiernagel, 2006). Ablation of ASEL and ASER were performed in N2 worms using positional cues. AIY was ablated in N2 worms. For genetic manipulation of AIY, we used OH8 *txx-3(mg158)* X, and OH161 *txx-3(ot22)* X.

Ablation of AIZ was performed in XL238 *ntIs5 [odr-2b3a::TN-XXL]* worms; the *odr-2b3a* promoter was a kind gift of the Colon-Ramos Lab. Ablation of SMB DL/VL and SMB DR/VR was performed in XL239 *ntIs10 [odr-2(18)::TN-XXL]* worms.

Laser ablation

Neurons were ablated as previously described (Bargmann and Avery, 1995). L1/L2 animals were mounted on 5% agarose pads containing 5-7mM of the anesthetic and paralytic agent NaN₃ before ablation of the neuron of interest with a focused laser beam. Sham ablated animals were mounted as described, but not subjected to the laser. Animals were recovered within 15 minutes of mounting and tested later as first-day adults.

Klinotaxis assay

Ablated animals and sham ablated controls were tested in the Y-chip microfluidic device as described (McCormick et al., 2011). Because klinotaxis expression can vary based on other environmental variables (e.g., temperature), ablated animals were compared to mock-ablated controls of the same genotype tested, in most cases, on the same day.

Solutions

In chemosensory experiments, the solutions contained (in mM) 1 CaCl₂, 1 MgSO₄, 10 HEPES, and NaCl as described in the text. The low-concentration solution had 0.001mM NaCl and the high-concentration solution had 50mM NaCl. Glycerol was

added to achieve a total osmolarity of 370 mOsm. All solutions were filtered with a pore size of 0.22 μm prior to use.

Data analysis and statistics

Image processing. The angle between the tip of the worms head and the longitudinal axis of the device was determined using the custom algorithms as described (McCormick et al., 2011).

Peak Amplitude. Peaks were identified using the Matlab Central script `peakdet` by user Eli Billauer (<http://billauer.co.il/peakdet.html>). The peak values during the 1 minute test epoch were averaged first by worm, and then the mean of worms was computed.

Cycle Duration. Duration was determined first by isolating individual cycles from the behavior during the test epoch, and then measuring the duration of the two hemi-cycles within it. The durations were averaged first by worm, and then the mean of worms was computed.

Integral. The integral was determined first by isolating individual cycles from the behavior during the test epoch, and then finding the area in the above zero portion and the below zero portion separately. The integrals were averaged first by worm, and then the mean of worms was computed.

Cycle Determination. We custom wrote a function to find upward-going zero crossings in plot of head angle over time. The function identifies potential cycle starts and ends, and then rejects cycles that are too short or too long and thus represent a behavior

other than well defined cyclic locomotion. Partial cycles were not included in duration and integral measures.

Statistics. To test the effects of concentration difference, I ran a one-way ANOVA with mean head angle and integral of the two hemi-cycles as dependent variables. Planned pairwise comparisons between groups were made using two-tailed Student's *t*-test. In ablation experiments, *t*-tests were run between ablated groups and sham ablated controls of the same genotype run in parallel. All *n* stated in figure legends refer to the number of worms rather than number of observations.

Laterality index

The laterality index was computed from the connectivity data published by wormatlas.org (<http://www.wormatlas.org/neuronalwiring.html#Connectivitydata>) Both mono- and poly-synaptic synapses were included. The index between any single neuron and a downstream neuron class was computed as follows:

$$L.I. = \frac{N_i}{N_i + N_c}$$

Where N_i is the number of ipsilateral synaptic contacts and N_c is the number of contralateral synaptic contacts.

CHAPTER IV

KLINOTAXIS IN CONTEXT: BROADENING THE NETWORK AND RELATING TO FREELY MOVING WORMS

MAIN TEXT

In the previous chapter, I explored the contribution of left- and right-sided members of a minimal network for klinotaxis. But how does this minimal network relate to the rest of the *C. elegans* nervous system? Do sensory neuron classes with similar preferred stimuli to the ASEs function to support the klinotaxis cycle in similar ways? Do any of the ablations tested result in changes to locomotion in the absence of a klinotaxis stimulus? What are the patterns of activity in the identified neurons in the network during klinotaxis? In this chapter, I address these questions by extending our ablation studies and beginning calcium imaging experiments.

I first expanded the minimal network addressed in Chapter III by investigating the other sensory neurons that function in klinokinesis and have been shown to respond with increases in intracellular calcium concentrations upon stimulation with sustained changes in sodium chloride concentration. Namely, the ADF left and right neurons have similar valence to the ASEL neurons and respond with increased calcium when $dC/dt > 0$ (ON cells, Thiele et al., 2009). Conversely, the ASH left and right neurons have similar valence to the ASER neurons and respond with increased calcium when $dC/dt < 0$ (OFF

cells, Thiele et al., 2009). The ADF sensory neurons impinge upon the minimal network previously investigated at both the interneuron and motor neuron levels. They make 1 synapse with AIY, 12 to AIZ, and 3 to the SMBs (Figure 1). The ASH sensory neurons do not have any chemical synaptic contacts with the interneurons or motor neurons of the minimal network, but they do make two electrical junctions with the AIZ neuron class. Interestingly, these connections also display ipsilateral bias. The ADF to AIZ synaptic contacts are perfectly ipsilateral, as are the gap junctions of ASH and AIZ: ASHL junctions with AIZL, and ASHR junctions with AIZR. However, we elected to examine the effects of the sensory neurons as bilateral pairs because of the calcium imaging evidence that these cells functionally overlap.

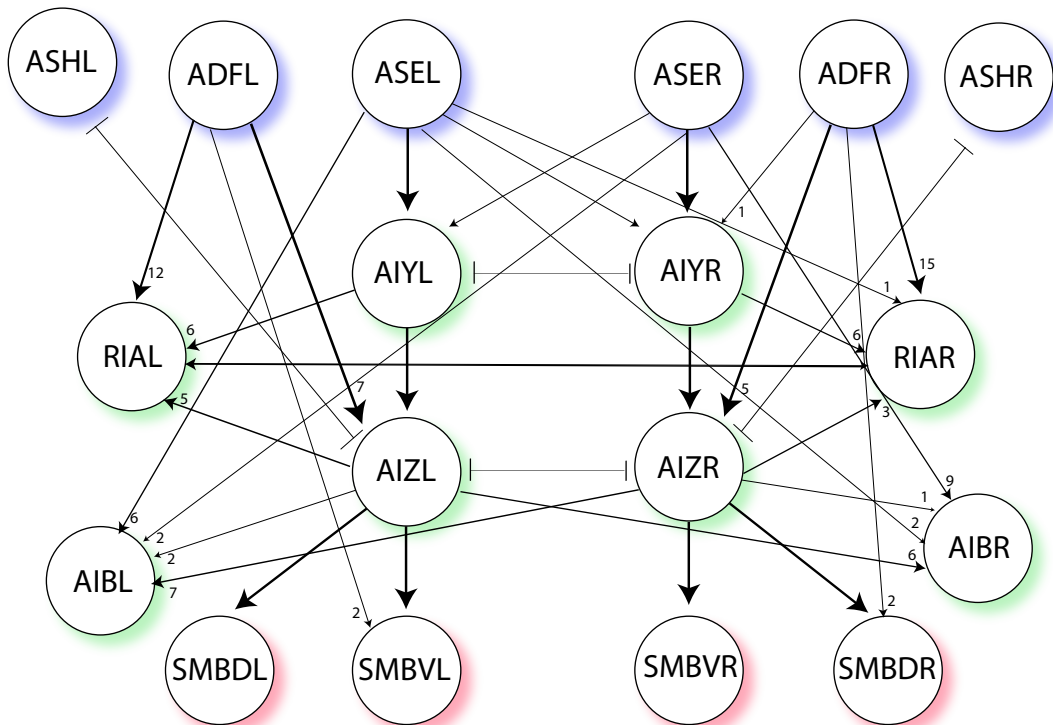
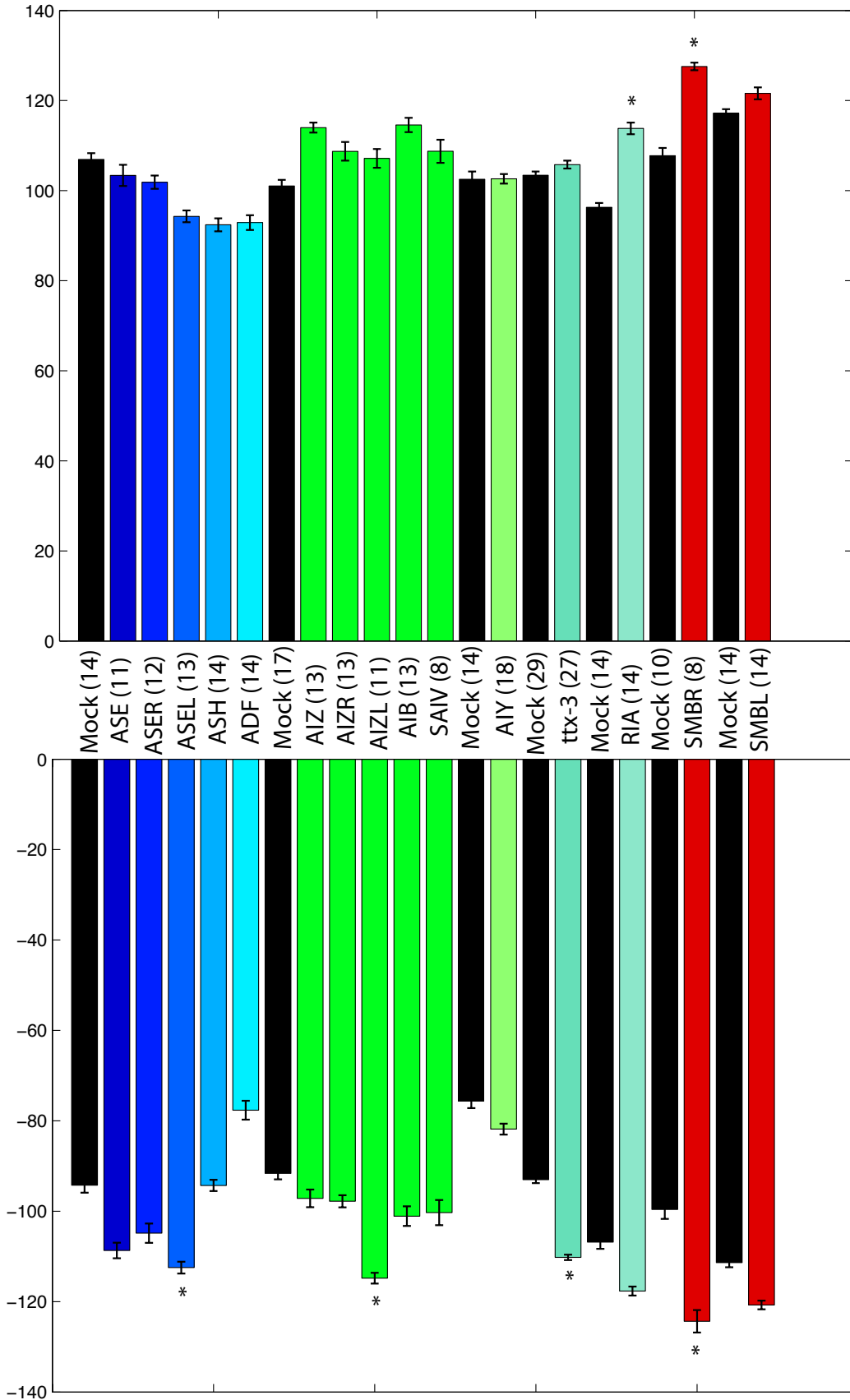


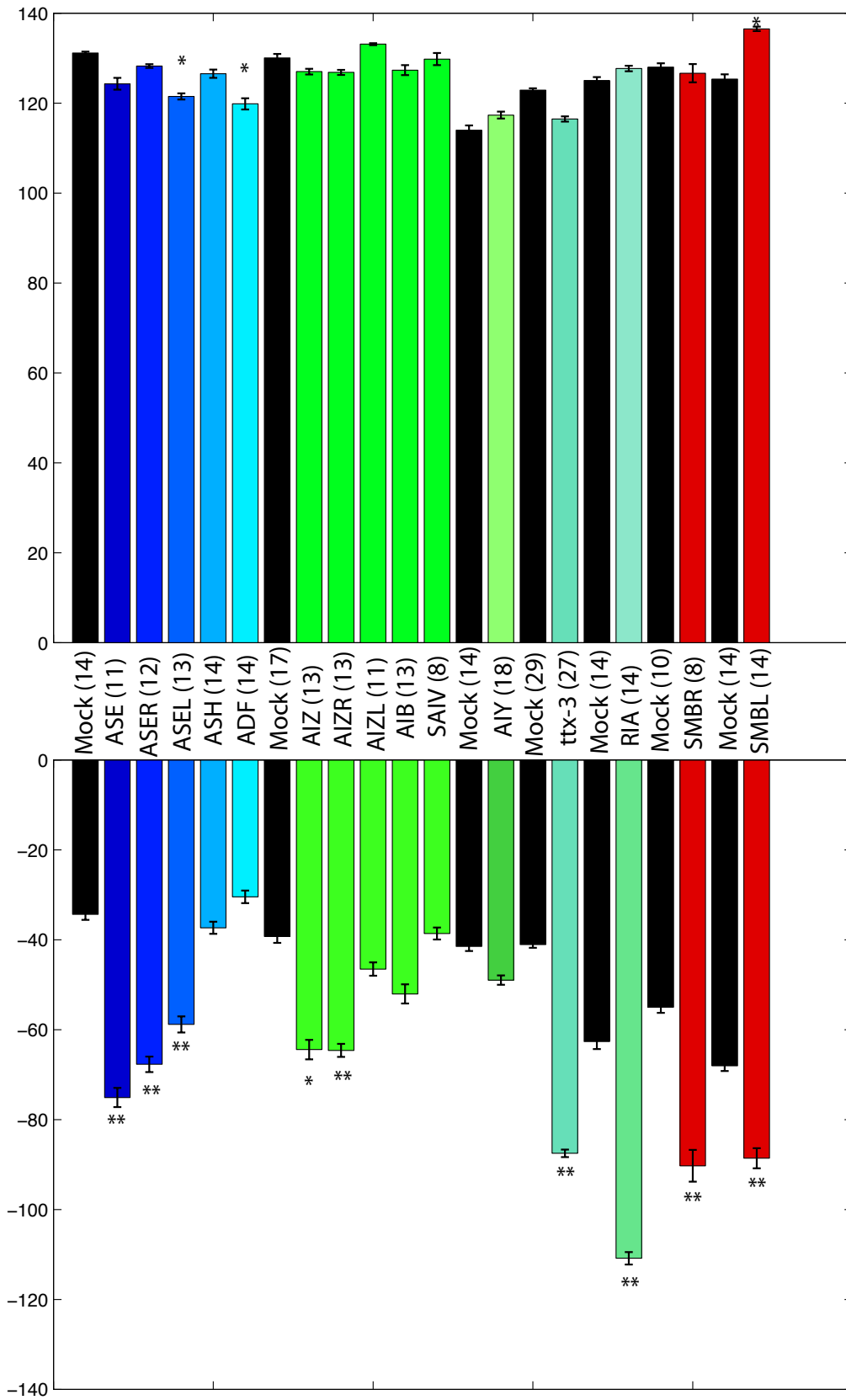
Figure 1. Extended neural network for klinotaxis, including putative sensory and interneurons. Blue shadow, sensory neurons. Green shadow, interneurons. Red shadow, motoneurons. Arrows represent synaptic connections, with number placed near the arrowhead. T's represent gap junctions.

For each ablation set, I analyzed the effect of ablation on the mean peak amplitude in the Y-chip using two stimulus conditions: 1) Symmetrical solutions of 0.001mM NaCl (Figure 2) and 2) Asymmetrical solutions with 50mM on one half and 0.001mM on the other (Figure 3). I hypothesized that ablation of SMBs would affect peak amplitude during baseline locomotion in symmetrical solutions, but predicted no other changes. I found that ablation of SMBRs led to increased amplitude on both sides of the undulation, but ablation of SMBLs did not. Other ablations also had significant effects on the peak amplitude on a single side of the undulation. The reason for this is not clear, but may be due to imperfect counterbalancing of the orientation of the animals within the device. Further analysis is need to determine the degree to which significant changes in amplitude during baseline conditions affect conclusions about the effects of a particular neuron during klinotaxis.

Figure 2. (next page) Summary of ablation experiments during symmetrical stimulus (0mM NaCl concentration difference). Mean peak amplitude is plotted along the abscissa. Positive values are arbitrarily assigned to the left side of the device. Blues bars, sensory neurons. Green bars, interneurons. Red bars, motor neurons. Error bars are S.E.M. * = $p < 0.05$. ** = $p < 0.01$.

Figure 3. (page after next) Summary of ablation experiments during asymmetrical stimulus (50mM NaCl concentration difference). Mean peak amplitude is plotted along the abscissa. Positive values, high-concentration peak. Negative values, low concentration peak. Blues bars, sensory neurons. Green bars, interneurons. Red bars, motor neurons. Error bars are S.E.M. * = $p < 0.05$. ** = $p < 0.01$.





During the asymmetrical stimulus used to elicit klinotaxis, I found that ablation of the ADF cells had effects similar to that of ablating ASEL. Namely, the peak amplitude of the portion of the locomotion cycle following an increase in concentration was reduced (Figure 3). These results indicate that ASEs are not the sole sensory neurons involved in klinotaxis. Ablation of ASH had no significant effects. The ADF neurons have a much stronger synaptic connection to the minimal network explored in the previous chapter than do the ASHs, and this may explain why we only found effects for ablation of ADF. AIZ interneurons in particular are one of the chief postsynaptic partners of the ADF class, eclipsed only by the RIA's with 27 synapses. Thus it is probable that the ADF class exerts its influence on klinotaxis through AIZs, although other possibilities can be imagined. The sensory function of ASH seem primarily to be for klinokinesis and not necessary for klinotaxis.

We next turned our attention to additional interneurons beyond the minimal network. We decided to investigate the AIB class because they exhibit sustained calcium responses to stepwise decreases in sodium chloride concentration (Oda et al., 2011). Both ASEs and AIZs have strong presynaptic projections to the AIB class, but AIBs have little input back to the minimal network: they have only 1 presynaptic projection to AIY and are not presynaptic to any other cell previously investigated. However, the possibility exists that the AIBs could impact klinotaxis through other inter- or motor neurons, e.g. the SMD motor neuron class. We found that ablation of AIBs had no significant effects on the klinotaxis locomotion cycle, as assayed by the peak amplitude of excursions in high- and

low-concentration regions. This result suggests that AIB interneurons function primarily in the neural network underlying klinokinesis rather than klinotaxis.

In 2012, Hendricks et al. published evidence that the interneuron class RIA has specialized subdomains present in its neurite that encode dorsal and ventral head deflections in separate compartments (Hendricks, 2012). This finding is fascinating and suggests a role for RIA in the klinotaxis network, as this neuron class has encoding mechanisms that could integrate sensory cell responses that encode the value of an action with motor or postural state, as required by the directed nature of klinotaxis. Additionally, as discussed above, the ADF sensory neuron class projects strongly to the RIA neurons and the ADF neuron is required for normal klinotaxis. The AIZ and AIY interneuron classes also project strongly to the RIA's (Figure 1). For these reasons, we decided to ablate the RIA neurons to investigate them for possible roles in klinotaxis. We found that RIA's are necessary for normal peak amplitude during both the high- and low-concentration regions of the locomotion cycle during klinotaxis in the microfluidic device (Figure 3). These results are exciting, but it is unclear how RIA is exerting its effects since it is not presynaptic to any of the neurons in the minimal network previously investigated. RIA's primary postsynaptic partner are the RMD motor neurons, with a whopping 86 synaptic contacts. In future work, we would like to investigate whether the RMD neuron class is also necessary for klinotaxis.

Beyond investigation via ablation studies, calcium imaging experiments can give complementary and corroborative evidence of the involvement of neurons underlying specific behaviors. Thus, I began to image from the neurons identified in the minimal

network ablation studies presented in the preceding chapter. Although the calcium responses of the ASE left and right neurons to sustained increases and decreases in sodium chloride concentration were already known, we decided to image during klinotaxis in the microfluidic device to determine if these calcium transients are present on the timescale of the locomotion cycle. We found that, as expected, the ASER neurons responded with high calcium during the portion of the locomotion cycle following a decrease in salt concentration (Figure 4), whereas the ASEL neurons responded with high calcium during the portion of the locomotion cycle following an increase in salt concentration (Figure 5). The cyclic nature of the underlying locomotion cycle makes these calcium dynamics cyclic during active klinotaxis. This raises the possibility that the absence of calcium in a sensory cell could be as salient a signal to a downstream neuron as the presence of calcium. This possibility may explain some of the mixed effects of ablation found in Chapter III for, e.g., the ASEL neuron.

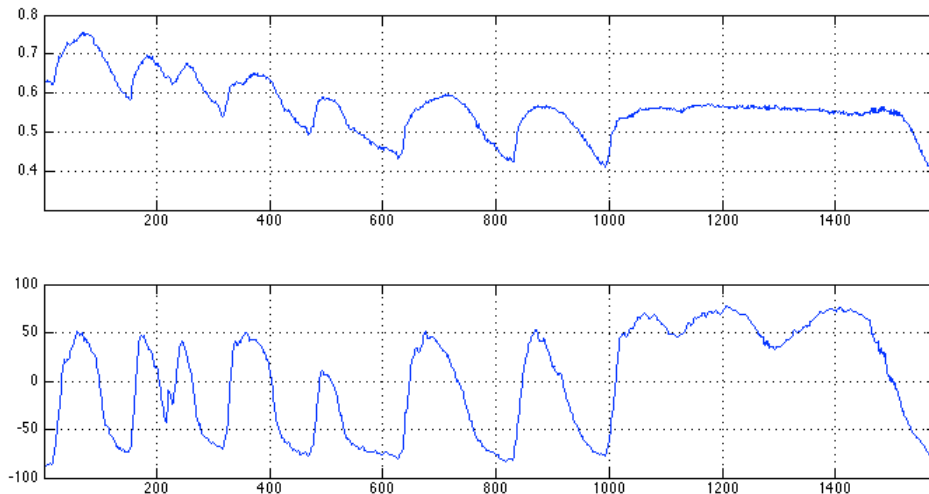


Figure 4. Calcium Imaging of ASER. Upper trace, ratio of CFP/YFP. Lower trace, head angle in degrees. High-concentration NaCl was present for positive head angles.

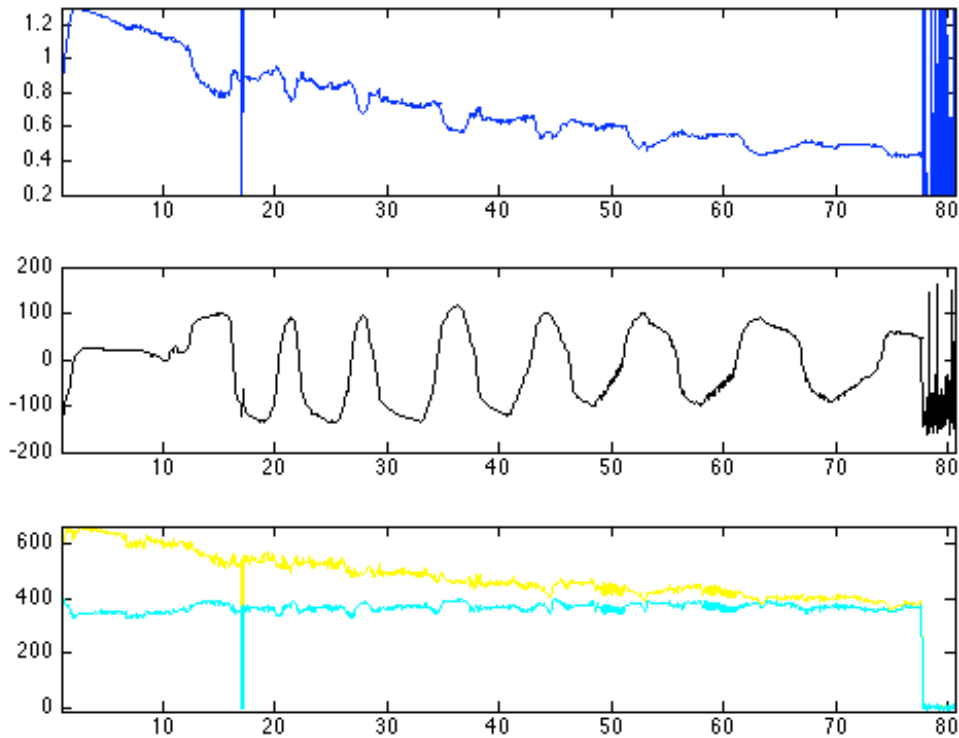


Figure 5. Calcium Imaging of ASEL. Upper trace, ratio of CFP/YFP representing relative calcium concentration. Middle trace, head angle in degrees. High-concentration NaCl was present for negative head angles. Lower trace, intensities of YFP and CFP, the two fluorophores in the calcium probe Cameleon used in this study, showing reciprocal changes.

ASER is the only sensory neuron identified to date that senses a decrease in chemoattractant concentration and is necessary for klinotaxis. The behavioral decrease in peak amplitude, duration, and integral of the portion of the locomotion cycle following a decrease in chemoattractant concentration is a key feature of klinotaxis. Using the light activated ion channel known as Channel Rhodopsin (ChR2), we investigated whether transient stimulation of the ASER neurons was sufficient to cause the noted behavioral decrease, in the absence of a concentration differential. We found anecdotal evidence that

photostimulation of the ASER neurons with brief pulses of blue light as the worm crossed the longitudinal axis of the Y-chip microfluidic device was sufficient to reduce the excursion in the direction the worm was heading at the time of photostimulation (Figure 6). Although this experiment requires repetition to be conclusive, it is a tantalizing bit of evidence that the activity of the ASER neuron is sufficient to drive klinotaxis.

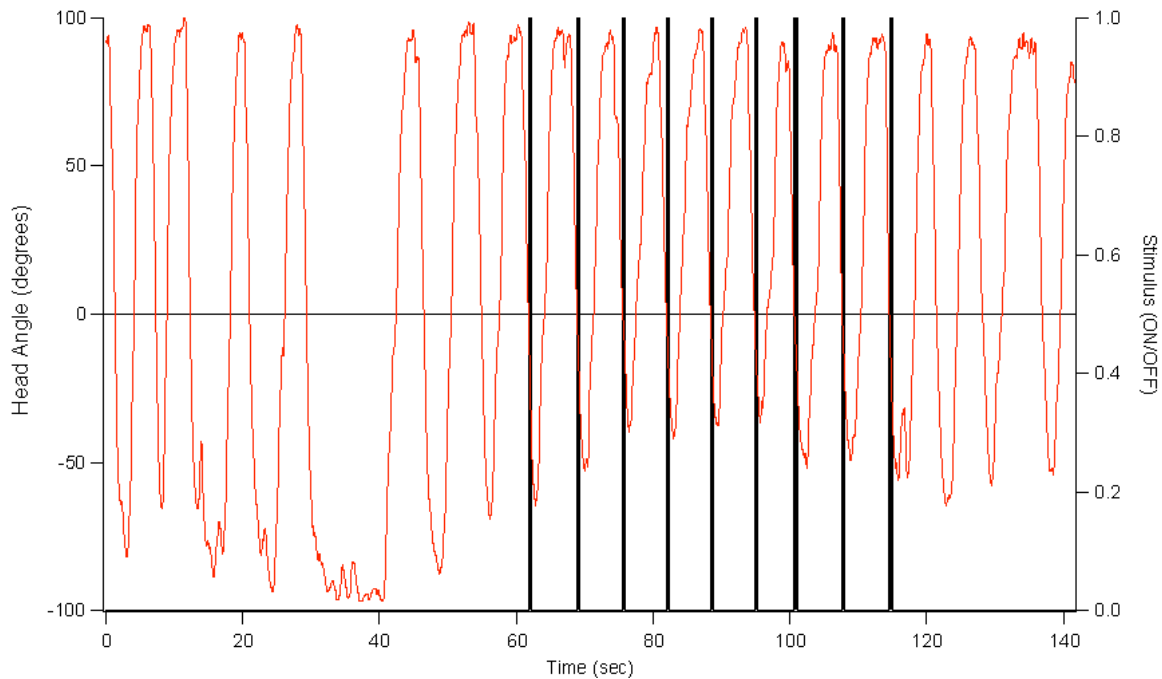


Figure 6. Photostimulation of ASER. Red trace, head angle in degrees. Black bars, timing of blue light stimulation.

Our studies of klinotaxis have relied heavily on the microfluidic device presented in Chapter II. This device is useful for giving the experimenter control over the stimuli presented to the worm, but it raises the question of how our studies of klinotaxis in a specialized microfluidic environment relate to studies of klinotaxis on agar plates. To partially address this question, I developed a model to translate the path taken by the worm in the device to a representation of what the path would look like if the worm were

freely moving. An example of this translation is presented in Figure 7. The model is adapted from the equations of motion governing the position of a theoretical worm (Izquierdo and Lockery, 2010, see Materials and Methods). The modeled path of the worm assuming the ability to translocate is what one might expect when considering the nature of the stimulus to which the worm was exposed. When the stimulus was a higher concentration of salt on the dorsal side of the worm, the worm turned in dorsal circles. Conversely, when the stimulus was a higher concentration of salt on the ventral side of the worm, the worm turned in ventral circles. Although the stimulus presented to the worm in the microfluidic device cannot be mapped onto the Euclidian plane, these results demonstrate that the bias to locomotion recorded in the device is qualitatively similar to the bias observed on agar plates in that both consist in a gradual curvature of the worms' forward going path.

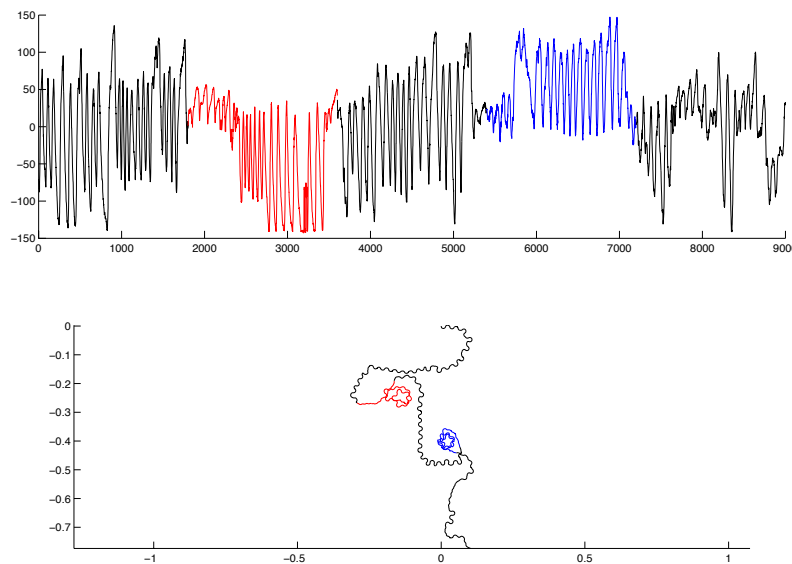


Figure 7. Modeling of worm tracks. Upper panel, head angle over time in the Y-chip. Lower panel, modeled worm tracks based on upper trace.

MATERIALS AND METHODS

Cultivation and strains

C. elegans were grown at 20° C on standard nematode growth medium (NGM) plates seeded with *E. coli* OP50 as described (Stiernagel, 2006). Ablation of ADF and ASH were performed in N2 worms using positional cues. Ablation of AIB was performed in XL238 *ntIs5 [odr-2b3a::TN-XXL]* worms . Ablation of RIA was performed in ZC1508 *yxIs19 [Pglr-3::GCaMP3, Punc-122::dsRed]* worms, a kind gift of Zhang Lab. Calcium imaging experiments were performed on XL228 *ntIs5; ntIs20 [Pflp-6::TN-XXL; pm6::TdTomato]* worms. Optogenetic experiments were performed on XL237 *ntIs1 [myo-2::tdTomato; gcy-5::Chr2 (#10)]; lite-1* worms.

Laser ablation

Neurons were ablated as previously described (Bargmann and Avery, 1995). L1/L2 animals were mounted on 5% agarose pads containing 5-7mM of the anesthetic and paralytic agent NaN₃ before ablation of the neuron of interest with a focused laser beam. Sham ablated animals were mounted as described, but not subjected to the laser. Animals were recovered within 15 minutes of mounting and tested later as first-day adults.

Behavioral assay

Ablated animals and sham ablated controls were tested in the Y-chip microfluidic device as described (McCormick et al., 2011). Sodium chloride was used as the

chemoattractant, with solutions containing 0.001 or 50mM NaCl, otherwise as previously described (McCormick et al, 2011).

Calcium imaging

Imaging experiments were performed on adult animals in the Y-chip microfluidic device (McCormick et al., 2011). Simultaneous tracking and imaging were performed as previously described (Faumont et al., 2011). The tracking target was tdTomato expressed in the sixth pharyngeal muscle cell layer (pm6::TdTomato), and was spectrally separated from the imaging target (flp-6::TN-XXL). Fluorescent images stacks were collected with HImage, and analysis was performed using custom MATLAB functions. Briefly, the cyan and citrine color channels were aligned via translation and rotation, and the region of interest was defined as a radius around the fluorescence emitted by the neuron of interest. Calcium signal is presented as a ratio of YFP/CFP, corrected for photobleaching.

Optogenetics

Worms were stimulated with a 400 ms pulse from a 535 nm laser as the tracking target (pm6) crossed the midline of the device. The pulse was automatically triggered via custom written IGOR scripts and microcontroller. The solution used was low-concentration NaCl in both arms of the microfluidic device.

Model parameters

The equations governing the motion of the theoretical worms were as follows:

$$p(t) = \left(\frac{dx}{dt}, \frac{dy}{dt} \right) = (v \cdot \cos(\mu(t)), v \cdot \sin(\mu(t)))$$

where $v(t)$ is 0.022 cm/s (0.0073 mm/frame) (Ferrée and Lockery, 1999) multiplied by a scaling factor to minimize the impact of small movements that may represent foraging or reversals:

$$v(t) = 0.0073 \cdot |\theta(t) - \theta(t-1)|$$

and

$$\mu(t) = \theta(t) + \sum_{i=1}^t b_i$$

where b_i is the mean of θ over a complete locomotion cycle at the conclusion of locomotion cycle and is otherwise 0. All θ values are converted to radians prior to computation.

CHAPTER V

CONCLUSION

After Samuel Ward's initial observation of worm behavior in 1973, Iino and Yoshida gave the first modern evidence of klinotaxis in their 2010 paper by tracking worms on agar plates that had been seeded with closely spaced bacterial lawns on a grid. They found evidence that animals change heading in a way that can be predicted by the concentration gradient perpendicular to their direction of motion. With ablation studies, they elucidate many of the neurons underlying this surprisingly efficient spatial orientation behavior, including the ASE and AIZ neuron classes. This work was the foundation of the work I undertook in this dissertation, and I owe it a great debt of gratitude.

I added to the body of knowledge on klinotaxis in *C. elegans* by designing a microfluidic device that separates the sensory environment on the dorsal and ventral sides of the worm. This device allows us to conclude that a difference in concentration between the lateral extremes of the worm's locomotive undulation cycle is sufficient to cause a bias to the worm's ongoing movement, and hence is a true klinotaxis. This device is versatile and can be broadly applied to other types of studies on *C. elegans*. This device represents a significant contribution to behavioral analysis in the *C. elegans* community.

I next investigated the neural basis of klinotaxis behavior, specifically with the hypothesis that the minimal neural network underlying this behavior displays left/right

asymmetry at all levels. I found evidence for this hypothesis in the wiring diagram and via ablation studies.

Finally, I extended the findings of the minimal network by broadening my ablation studies to other potentially necessary sensory and interneurons. I found that the ADF and RIA neurons are also necessary for normal klinotaxis. Additionally, I imaged from the ASE sensory neurons during klinotaxis in the microfluidic chip and found that they were active on the time scale of the locomotion cycles that are the foundation of the klinotaxis concentration comparison. I present anecdotal evidence that the activity of the ASER neuron is sufficient to generate klinotaxis behavior, and present a model to translate behavior recorded in the microfluidic device to the path of a freely moving animal.

Although these studies were not exhaustive, and there is yet more to discover about the neuronal basis of klinotaxis in *C. elegans*, my dissertation represents a significant step forward in that it investigates a complete sensorimotor transformation of a fully connected network that is implicated in this behavior.

REFERENCES CITED

- Adler J (1966) Chemotaxis in bacteria. *Science* 153: 708-716.
- Ahmed T, Shimizu TS, Stocker R (2010) Microfluidics for bacterial chemotaxis. *Integr. Biol. (Camb)* 2: 604-629.
- Albrecht DR, Bargmann CI (2011) High-content behavioral analysis of *Caenorhabditis elegans* in precise spatiotemporal chemical environments. *Nat. Methods* 8(7): 599-605.
- Altun-Gultekin Z, Andachi Y, Tsalik EL, Pilgrim D, Kohara Y, Hobert O (2001) A regulatory cascade of three homeobox genes, *ceh-10*, *ttx-3* and *ceh-23*, controls cell fate specification of a defined interneuron class in *C. elegans*. *Development* 128(11): 1951-69.
- Ardiel EL, Rankin CH (2010) An elegant mind: learning and memory in *Caenorhabditis elegans*. *Learn. Mem.* 17: 191-201.
- Bargmann CI (2006) Chemosensation in *C. elegans*. *WormBook*: 1-29.
- Bargmann CI, Horvitz HR (1991) Chemosensory neurons with overlapping functions direct chemotaxis to multiple chemicals in *C. elegans*. *Neuron* 7: 729-742.
- Bargmann CI, Avery L (1995) Laser killing of cells in *Caenorhabditis elegans*. *Methods Cell Biol.* 48: 225-250.
- Ben-Yakar A, Chronis N, Lu H (2009) Microfluidics for the analysis of behavior, nerve regeneration, and neural cell biology in *C. elegans*. *Curr. Opin. Neurobiol.* 19: 561-567.
- Berg HC, Brown DA (1972) Chemotaxis in *Escherichia coli* analysed by three-dimensional tracking. *Nature.* 239(5374): 500-504.
- Brenner, S (1974) The genetics of *Caenorhabditis elegans*. *Genetics* 77: 71-94.
- Bretscher AJ, Kodama-Namba E, Busch KE, Murphy RJ, Soltesz Z, Laurent P, deBono M (2011) Temperature, oxygen, and salt-sensing neurons in *C. elegans* are carbon dioxide sensors that control avoidance behavior. *Neuron* 69: 1099-1113.

- Chalfie M, Tu Y, Euskirchen G, Ward WW, Prasher DC (1994) Green fluorescent protein as a marker for gene expression. *Science* 263(5148): 802-805.
- Chang S, Johnston RJ Jr, Hobert O (2003) A transcriptional regulatory cascade that controls left/right asymmetry in chemosensory neurons of *C. elegans*. *Genes Dev.* 17(17): 2123-2137.
- Chen BL, Hall DH, Chklovskii DB (2006) Wiring optimization can relate neuronal structure and function. *Proc. Natl. Acad. Sci. U.S.A.* 103(12): 4723-4278.
- Chokshi TV, Bazopoulou D, Chronis N (2010) An automated microfluidic platform for calcium imaging of chemosensory neurons in *Caenorhabditis elegans*. *Lab Chip* 10: 2758-2763.
- Croll NA (1975a) Components and patterns in the behavior of the nematode *Caenorhabditis elegans*. *J. Zool.* 176:159–176.
- Croll NA (1975b) Behavioral analysis of nematode movement. *Adv. Parasitol.* 13:71–122.
- Culotti J, Russell R (1978) Osmotic avoidance defective mutants of the nematode *C. elegans*. *Genetics* 90: 243-256.
- Dunn G (1990) Conceptual problems with kinesis and taxis. in *Biology of the chemotactic response*, eds Armitage JP, Lackie JM (Cambridge UP, Cambridge, U.K.) 1–13.
- Dusenbury DB (1974) Analysis of chemotaxis in the nematode *Caenorhabditis elegans* by countercurrent separation. *J. Exp. Zool.* 188(1): 41-47.
- Dusenbury DB, Sheridan RE, Russell RL (1975) Chemotaxis-defective mutants of the nematode *Caenorhabditis elegans*. *Genetics* 80: 297-309.
- Fraenkel GS, Gunn DL (1940) *The Orientation of Animals*. Oxford: Oxford University Press.
- Faumont S, Miller AC, Lockery SR (2005) Chemosensory behavior of semi-restrained *Caenorhabditis elegans*. *J. Neurobiol.* 65: 171-178.
- Faumont S, Lockery SR (2006) The awake behaving worm: simultaneous imaging of neuronal activity and behavior in intact animals at millimeter scale. *J. Neurophysiol.* 95: 1976-1981.

- Faumont S, Rondeau G, Thiele TR, Lawton KJ, McCormick KE, et al. (2011) An image-free opto-mechanical system for creating virtual environments and imaging neuronal activity in freely moving *Caenorhabditis elegans*. *PLoS ONE* 6(9): e24666.
- Faumont S, Lindsay TH, Lockery SR (2012) Neuronal microcircuits for decision making in *C. elegans*. *Curr. Opin. Neurobiol.* 4: 580-591.
- Garrity PA, Goodman MB, Samuel AD, Sengupta P (2010) Running hot and cold: behavioral strategies, neural circuits, and the molecular machinery for thermotaxis in *C. elegans* and *Drosophila*. *Genes Dev.* 24: 2365-2382.
- Giuffre C, Hinow P, Vogel R, Ahmed T, Stocker R, et al. (2011) The ciliate *Paramecium* shows higher motility in non-uniform chemical landscapes. *PLoS ONE* 6: e15274.
- Gray JM, Karow DS, Lu H, Chang AJ, Chang JS, et al. (2004) Oxygen sensation and social feeding mediated by a *C. elegans* guanylate cyclase homologue. *Nature* 430: 317-322.
- Gray JM, Chalasani SK, Bargmann CI (2005) A circuit for navigation in *Caenorhabditis elegans*. *102(9): 3184:91.*
- Gomez-Marin A, Duistermars BJ, Frye MA, Louis M (2010) Mechanisms of odor-tracking: multiple sensors for enhanced perception and behavior. *Front Cell Neurosci.* 4:6.
- Gomez-Marin A, Stephens GJ, Louis M (2011) Active sampling and decision making in *Drosophila* chemotaxis. *Nat. Commun.* 2:441.
- Hall DH, Alutun ZF (2008) *C. elegans* atlas. Woodbury: Cold Spring Harbor Laboratory Press.
- Hedgecock EM, Russell RL (1975) Normal and mutant thermotaxis in the nematode *Caenorhabditis elegans*. *Proceedings of the National Academy of Science* 72: 4061-4065.
- Hendricks M, Ha H, Maffey N, Zhang Y. (2012) Compartmentalized calcium dynamics in *C. elegans* interneuron encode head movement. *Nature* 487(7405): 99-103.

- Hilliard MA, Bargmann CI, Bazzicalupo P (2002) *C. elegans* responds to chemical repellents by integrating sensory inputs from the head and the tail. *Curr. Biol.* 12: 730-734.
- Hobert O (2004) Common logic of transcription factor and microRNA action. *Trends Biochem. Sci.* 9: 462-8.
- Iino Y, Yoshida K (2009) Parallel use of two behavioral mechanisms for chemotaxis in *Caenorhabditis elegans*. *J. Neurosci.* 29: 5370-5380.
- Ito H, Inada H, Mori I (2006) Quantitative analysis of thermotaxis in the nematode *Caenorhabditis elegans*. *J. Neurosci. Methods* 154: 45-52.
- Izquierdo EJ, Lockery SR (2010) Evolution and Analysis of Minimal Neural Circuits for Klinotaxis in *Caenorhabditis elegans*. *J. Neurosci.* 30: 12908-12917.
- Izquierdo EJ, Beer R (2013) Connecting a connectome to behavior: an ensemble of neuroanatomical models of *C. elegans* klinotaxis. *PLoS Comput. Biol.* 9(2): e1002890.
- Jeon NL, Dertinger SKW, Chiu DT, Choi IS, Stroock AD, et al. (2000) Generation of solution and surface gradients using microfluidic systems. *Langmuir* 16: 8311-8316.
- Jurado P, Kodama E, Tanizawa Y, Mori I (2010) Distinct thermal migration behaviors in response to different thermal gradients in *Caenorhabditis elegans*. *Genes Brain Behav.* 9: 120-127.
- Kandel ER, Schwartz JH, Jessell TM (2000) Principles of Neural Science, McGraw Hill.
- Kerr R, Lev-Ram V, Baird G, Vincent P, Tsien RY, Schafer WR (2000) Optical imaging of calcium transients in neurons and pharyngeal muscle of *C. elegans*. *Neuron* 3: 583-94.
- Komatsu J, Mori I, Rhee J-S, Akaike N, Ohshima Y (1996) Mutations in a cyclic nucleotide-gated channel lead to abnormal thermosensation and chemosensation in *C. elegans*. *Neuron* 17: 707-718.
- Koyama S, Amarie D, Soini HA, Novotny MV, Jacobson SC (2006) Chemotaxis assays of mouse sperm on microfluidic devices. *Anal. Chem.* 78: 3354-3359.

- Leifer AM, Fang-Yen C, Gershow M, Alkema MJ, Samuel AD (2011) Optogenetic manipulation of neural activity in freely moving *Caenorhabditis elegans*. *Nat. Methods* 8: 147-152.
- Lindell AK (2013) Continuities in emotion lateralization in human and non-human primates. *Front. Hum. Neurosci.* 7: 464.
- Lockery SR, Lawton KJ, Doll JC, Faumont S, Coulthard SM, et al. (2008) Artificial Dirt: microfluidic substrates for nematode neurobiology and behavior. *J. Neurophysiol.* 99: 3136-3143.
- Lockery SR (2011) The computational worm: spatial orientation and its neuronal basis in *C. elegans*. *Curr. Opin. Neurobiol.* 21(5) : 782-790.
- Mathewson RF, Hodgeson ES (1972) Klinotaxis and rheotaxis in orientation of sharks toward chemical stimuli. *Comp. Biochem. Physiol. A. Comp. Physiol.* 42(1): 79:84.
- McCormick KE, Gaertner BE, Sotile M, Phillips P, and Lockery SR (2011) Microfluidic devices for analysis of spatial orientation in semi-restrained *C. elegans*. *PLoS ONE* 6(10): e25710.
- Oda S, Tomioka M, Iino Y (2011) Neuronal plasticity regulated by the insulin-like signaling pathway underlies salt chemotaxis learning in *Caenorhabditis elegans*. *J. Neurophysiol.* 106(1): 301-308.
- Oklenburg S, Güntürkün O. (2012) Hemispheric Asymmetries: The Comparative View. *Front. Psychol.* 3: 5.
- Pierce-Shimomura JT, Morse TM, Lockery SR (1999) The fundamental role of pirouettes in *Caenorhabditis elegans* chemotaxis. *J. Neurosci.* 19: 9557-9569.
- Pierce-Shimomura JT, Chen BL, Mun JJ, Ho R, Sarkis R, et al. (2008) Genetic analysis of crawling and swimming locomotory patterns in *C. elegans*. *Proc. Natl. Acad. Sci. U.S.A.* 105: 20982-20987.
- Porter J, Craven B, Khan RM, Chang SJ, Kang I, et al. (2007) Mechanisms of scent-tracking in humans. *Nat. Neurosci.* 10: 27-29.
- Qin D, Xia Y, Whitesides GM (2010) Soft lithography for micro- and nanoscale patterning. *Nat. Protoc.* 5: 491-502.

- Ramot D, MacInnis BL, Lee HC, Goodman MB (2008) Thermotaxis is a robust mechanism for thermoregulation in *Caenorhabditis elegans* nematodes. *J. Neurosci.* 28: 12546-12557.
- Remy JJ, Hobert O (2005) An interneuronal chemoreceptor required for olfactory imprinting in *C. elegans*. *Science* 309(5735): 787-90.
- Riddle DL, Blumenthal T, Meyer BJ, Priess JR (1997) *C. elegans* II. Plainview: Cold Spring Harbor Laboratory Press.
- Ryu WS, Samuel AD (2002) Thermotaxis in *Caenorhabditis elegans* analyzed by measuring responses to defined thermal stimuli. *J. Neurosci.* 22: 5727-5733.
- Sambongi Y, Nagae T, Liu Y, Yoshimizu T, Takeda K, et al. (1999) Sensing of cadmium and copper ions by externally exposed ADL, ASE, and ASH neurons elicits avoidance response in *Caenorhabditis elegans*. *Neuroreport* 10: 753-757.
- Stiernagle T (2006) Maintenance of *C. elegans*. *WormBook*: 1-11.
- Stirman JN, Crane MM, Husson SJ, Wabnig S, Schultheis C, et al. (2011) Real-time multimodal optical control of neurons and muscles in freely behaving *Caenorhabditis elegans*. *Nat. Methods* 8: 153-158.
- Suzuki H, Thiele TR, Faumont S, Ezcurra M, Lockery SR, Schaffer WR (2008) Functional Asymmetry in *Caenorhabditis elegans* taste neurons and its computational role in chemotaxis. *Nature* 454 (7200): 114-7.
- Taylor RW, Hsieh YW, Gamse JT, Chuang CF (2010) Making a difference together: reciprocal interactions in *C. elegans* and zebrafish asymmetric neural development. *Development* 137, 681–691.
- Thiele TR, Faumont S, Lockery SR (2008) The neural network for chemotaxis to tastants in *Caenorhabditis elegans* is specialized for temporal differentiation. *J. Neurosci.* 29(38): 11904:11.
- Vallortigara G, Rogers LJ (2005) Survival with an asymmetrical brain: advantages and disadvantages of cerebral lateralization. *Behav. Brain Sci.* 28(4): 575-89.

- Ward S (1973) Chemotaxis by the nematode *Caenorhabditis elegans*: identification of attractants and analysis of the response by use of mutants. *Proc. Natl. Acad. Sci. U.S.A.* 70: 817-821.
- Ward S, Thomson N, White JG, Brenner S (1975) Electron microscopical reconstruction of the anterior sensory anatomy of the nematode *Caenorhabditis elegans*. *J. Comp. Neurol.* 160:313–338.
- White, J. G., Southgate, E., Thomson, J. N. & Brenner, S (1986) The structure of the nervous system of the nematode *Caenorhabditis elegans*. *Philos. Trans. R. Soc. Lond., B, Biol. Sci.* 314, 1–340.
- White JQ, Nicholas TJ, Gritton J, Truong L, Davidson ER, et al. (2007) The sensory circuitry for sexual attraction in *C. elegans* males. *Curr. Biol.* 17: 1847-1857.
- Wicks SR, de Vries CJ, van Luenen HG, Plasterk RH (2000) CHE-3, a cytosolic dynein heavy chain, is required for sensory cilia structure and function in *Caenorhabditis elegans*. *Dev. Biol.* 221: 295-307.
- Zariwala HA, Miller AC, Faumont S, Lockery SR (2003) Step response analysis of thermotaxis in *Caenorhabditis elegans*. *J. Neurosci.* 23: 4369-4377.